




Brain Connectivity for Diagnosis and Treatment

Hamid Soltanian-Zadeh * 

Control and Intelligent Processing Center of Excellence, School of Electrical and Computer Engineering, College of Engineering, University of Tehran, Tehran, Iran

*Corresponding Author: Hamid Soltanian-Zadeh
Email: hszadeh@ut.ac.ir

Abstract

Estimation of brain connectivity, as a brain mapping technique, has become increasingly important in the diagnosis and treatment of neurological and psychiatric disorders. Understanding how different regions of the brain communicate with each other provides valuable insights into the underlying mechanisms of these conditions. Brain connectivity includes structural connectivity and functional connectivity and can be utilized in various scenarios for diagnosis, treatment, and prognosis of mental disorders. This editorial briefly presents structural and functional brain connectivity and some of their applications.

Keywords: Brain Connectivity; Brain Stimulation; Neurosurgical Planning; Brain Mapping; Artificial Intelligence.

1. Diagnosis

Functional Connectivity (FC): Aberrant patterns of functional connectivity, estimated from the resting-state fMRI or task-based fMRI, can serve as biomarkers of various disorders. Functional connectivity patterns may be indicative of conditions such as schizophrenia, depression, and Attention Deficit Hyperactivity Disorder (ADHD).

Structural Connectivity (SC): Disruptions in white matter tracts, identified through Diffusion Tensor Imaging (DTI) and quantified by structural connectivity metrics, can be associated with neurodegenerative diseases such as Alzheimer's and multiple sclerosis.

2. Disease Subtyping

Brain connectivity analysis can contribute to the identification of subtypes within a broader disorder. For example, in psychiatric disorders like schizophrenia, distinct connectivity patterns may be associated with different symptom profiles, aiding in more personalized treatment strategies.

3. Prediction of Treatment Effect

Functional Connectivity Changes: Monitoring changes in functional connectivity before and after treatment can help predict treatment response. For instance, alterations in brain connectivity may be observed following interventions such as psychotherapy or medication.

Neurofeedback: Real-time monitoring of brain connectivity through neurofeedback can be used to guide and enhance therapeutic interventions. Patients can learn to modulate their brain activity based on feedback received during neuroimaging.

4. Brain Stimulation

Brain connectivity information is crucial in the application of non-invasive brain stimulation techniques such as Transcranial Magnetic Stimulation (TMS) or transcranial Direct Current Stimulation (tDCS). Targeting specific brain regions based on

connectivity patterns can optimize the effectiveness of these treatments.

5. Neurosurgical Planning

Prior to neurosurgical procedures such as those directed towards treatment of epilepsy and brain tumors, mapping of the functional and structural connectivity helps surgeons avoid critical areas and minimize the risk of postoperative deficits.

6. Monitoring Progression

Longitudinal studies using connectivity measures allow researchers and clinicians to track the progression of neurological disorders over time. This information is vital for understanding disease trajectories and optimizing intervention strategies.

7. Integrative Approaches

Combining information from multiple neuroimaging modalities such as structural MRI, functional MRI, and DTI provides a more comprehensive view of the brain connectivity, offering a holistic understanding of the brain's organization and function.

8. AI-Based Methods

While brain connectivity analysis holds great promise, the field is still evolving, and further research is needed to develop novel analysis approaches and establish standardized protocols and enhance the clinical utility of these measures. To this end, Artificial Intelligence (AI) based techniques will play a significant role in advancing brain connectivity analysis by providing sophisticated tools for data processing, feature extraction, and interpretation, as described below.

Preprocessing: AI algorithms can automate the preprocessing of neuroimaging data, handling tasks such as motion correction, normalization, and noise reduction. This ensures that the data used for connectivity analysis is of high quality.

Identifying Connectivity Patterns: AI techniques, particularly machine learning algorithms, can extract complex patterns of connectivity from large datasets. These patterns may not be readily apparent through traditional analyses, allowing for a more nuanced understanding of the brain networks.

Reducing Dimensionality: AI methods help manage the high dimensionality of neuroimaging data by identifying the most relevant features. This is crucial for reducing computational complexity and improving the interpretability of results.

Identifying Disease Biomarkers: AI algorithms can identify subtle connectivity patterns associated with specific neurological or psychiatric disorders. This enables the development of potential biomarkers for diagnostic purposes.

Predicting Treatment Response: Machine learning models can analyze connectivity data to predict how an individual might respond to a particular treatment, facilitating personalized and targeted therapeutic interventions.

Combining Imaging Modalities: AI facilitates the integration of data from different imaging modalities, such as structural MRI, functional MRI, and DTI. This multimodal approach provides a more comprehensive understanding of brain connectivity.

Enhancing Real-Time Neurofeedback: AI algorithms can be employed in real-time neurofeedback systems, allowing individuals to modulate their brain activity based on ongoing connectivity patterns. This is particularly relevant in therapeutic interventions and cognitive training.

Identifying Disease Subtypes: AI methods can uncover subtypes within larger patient populations based on connectivity patterns. This can aid in personalized medicine by tailoring treatments to specific subgroups.

Predictive Modeling: AI models can predict clinical outcomes or disease progression based on connectivity data. This information is valuable for prognosis and long-term treatment planning.

Quality Control: AI algorithms assist in quality control by automatically flagging problematic data points or outliers, ensuring that only reliable data contribute to the analysis.

Big Data: AI is instrumental in handling large-scale datasets commonly encountered in neuroimaging studies. This includes efficient storage, retrieval, and analysis of big data, promoting collaborative research efforts.

Optimizing Brain Stimulation: In applications such as non-invasive brain stimulation, AI can optimize the targeting of specific brain regions by considering individual variability in connectivity patterns.

While AI has shown great promise in advancing brain connectivity analysis, ongoing research and validation are essential to ensure the reliability and generalizability of AI-driven findings in clinical contexts. Moreover, ethical considerations, data privacy, and transparency in AI algorithms are crucial aspects that need careful attention in neuroimaging research.

9. ISBM 2023

Many of the connectivity approaches and applications discussed above have been used and discussed in the speeches, panels, and papers presented in the Seventh Iranian Symposium of Brain Mapping Updates (ISBM'2023). The papers presented at the symposium and published in this Special Issue have been reviewed by experts in the field and were the best among the submitted papers. They describe specific approaches for the analysis of neuroimaging data or specific applications of neuroimaging, brain mapping, and brain connectivity analysis techniques for the diagnosis and treatment of the brain disorders.



The Legacy of War: How Trauma Affects Empathy in Future Generations

Mandana Sajjadi^{1*} , Hossein Salimi¹, Mohammad Taghi Joghataei², Soraya Mehrabi³

¹Department of International Relations, Faculty of Law and Political Sciences, Allameh Tabataba'i University, Tehran, Iran

²Department of Anatomy, School of Medicine, Iran University of Medical Sciences, Tehran, Iran

³Department of Physiology, Faculty of Medicine, Iran University of Medical Sciences, Tehran, Iran

*Corresponding Author: Mandana Sajjadi

Email: Sajjadiatu@gmail.com

Abstract

Empathy towards out-groups is essential for maintaining peaceful and favourable relationships with other nations. The experience of war can damage the empathy between two nations. New developments in trauma studies reveal that the impacts of war can be inherited. This study investigated whether war experiences impact future generations' ability to empathize with out-groups with negative experiences. In this fMRI study, 30 healthy participants (15 individuals with a family history of trauma from the Iran and Iraq wars and 15 controls) viewed video clips of Iraqi, Afghan, and Iranian patients displaying facial expressions of pain. Next, they were asked to rate the level of distress shown. Participants from families not affected by war exhibit more empathy-related brain activity when watching videos of Iraqi patients. The affected regions are the corpus callosum, limbic and hippocampal areas, and, partially, the prefrontal lobe. Participants from the main group showed increased activity in the occipital lobe when watching Iraqi pain and insula regions when viewing video clips of the suffering of Irani patients, indicating a stronger response to unpleasant images and a preference for their group. The research found that war trauma negatively affects the next generation's empathetic feelings toward hostile ethnic groups.

Keywords: Intergenerational Transmission of Trauma; War Trauma; Empathy; Outgroup Bias; functional Magnetic Resonance Imaging Study.

1. Introduction

The experience of war can be traumatic and have lasting effects, not just on those who directly experience it but also on future generations. Neuroscience has made significant progress in understanding the neural processes associated with war trauma and empathy, showing how these experiences can negatively impact survivors' ability to understand others' perspectives [1-4]. Determining the stability of these effects among future generations of society requires further research. Thus, our study focused on determining whether the offspring of Iran-Iraq war survivors with a history of war trauma exhibit reduced empathy towards Iraqis.

War-time stress can affect children indirectly. These effects can be long-lasting and may persist until the individual's lifetime. Reviewing the literature on "Intergenerational Transmission of Trauma" confirms that the consequences of this disorder in parents are transmitted to children through various mechanisms. [5-9]. Recent studies suggest that war-induced trauma also impacts children biologically. New molecular biology studies have confirmed that traumatic injuries' effects can be transmitted to the first to fourth generation through epigenetic mechanisms. These mechanisms change the DNA transcript [10-13]. It has been discovered that the transmission of PTSD to children is linked to biological changes in the Hypothalamic-Pituitary-Adrenal axis (HPA). According to Decety (2011), the HPA axis is a component of the neural system that represents empathy. We can anticipate differences in how empathy is demonstrated among children with war-related trauma family backgrounds.

2. Materials and Methods

2.1. Participants

Thirty healthy Iranian participants (18 males), all right-handed, with a mean age of 30 years ($SD=3$), provided written consent for the fMRI experiment. The Ethics Committee of Allameh Tabataba'i University authorized the research (IR.ATU.REC.1399.056). Participants had no neurological or psychiatric disorders, were not taking

medication, and had normal or corrected-normal vision. They were compensated for their participation.

2.2. General Procedure

In order to ensure the success of our experiment, we were very selective in the initial stages of participant recruitment. Six months before the fMRI experiment, we distributed questionnaires to 536 individuals born in the 1980s and 1990s and were the first-generation offspring of Iran-Iraq war survivors. We used the Interpersonal Reactivity Index [14] to identify individuals with above-average levels of empathy. To determine the influence of parental socioeconomic status and education on child-rearing, we used the Socioeconomic Status Questionnaire (2012). Additionally, we used Bernstein et al.'s [15] childhood trauma questionnaire (2003) to assess the impact of childhood trauma. As part of the survey, participants were also asked to rate their family's political leanings during their childhood on a scale of 0 to 10, ranging from reformist to extremely conservative. We created a questionnaire to understand how severe parents' traumatic experiences were from their children's perspective. The questionnaire was inspired by a similar study conducted in 2006 among children of Holocaust survivors. Yehuda et al. [16] designed a brief questionnaire that assessed parents' post-traumatic stress disorder symptoms from the children's viewpoint. Our questionnaire helped us understand how much exposure the children had to their family's trauma narratives, observed symptoms, or experienced consequences. The questionnaire's validity was confirmed to be 0.81 Cronbach's alpha. As part of our survey, we included two open-ended questions for children to share their parent's experiences during the Iran-Iraq war. We evaluated parents' traumatic experiences by assessing the type and severity of situations they faced, such as war zones, forced migration, bombardment anxiety, having veteran family members, mental and emotional distress, and time spent at the front. 16 main-group participants (8 males) with severe family trauma and 14 control participants (10 males) without a family record of war trauma were selected for an fMRI test.

2.3. Visual Stimuli

We utilized a video clip to examine empathy for pain and out-group biases. The participants watched patients of different ethnicities (Iranians, Afghans, and Iraqis) displaying expressions of pain on their faces, which progressed from neutral to intense pain expression. The selection of stimuli was influenced by previous research [17, 18]. International student volunteers from Allameh Tabatabai University were taught to express pain through specific facial expressions, such as frowning and pressing their lips [19].

The group consisted of 34 Iraqis, 44 Iranians, and 32 Afghans, and the final version was recorded after multiple trial recordings. The videos were captured using a stable tripod to prevent shaking and filmed from a front-facing angle that shows people's faces and part of their shoulders (Figure 1). The individuals in the videos were instructed to focus on a point 50 cm below the camera to avoid direct eye contact with the audience. To make the hospital scenes more realistic, the actors wore regular clothes and stood against a white wall. Each video lasted 8 seconds, with the first 0.5 seconds being neutral expressions and the remaining 7.5 seconds showing pain caused by audio. From all the videos, 48 clips that showed the most

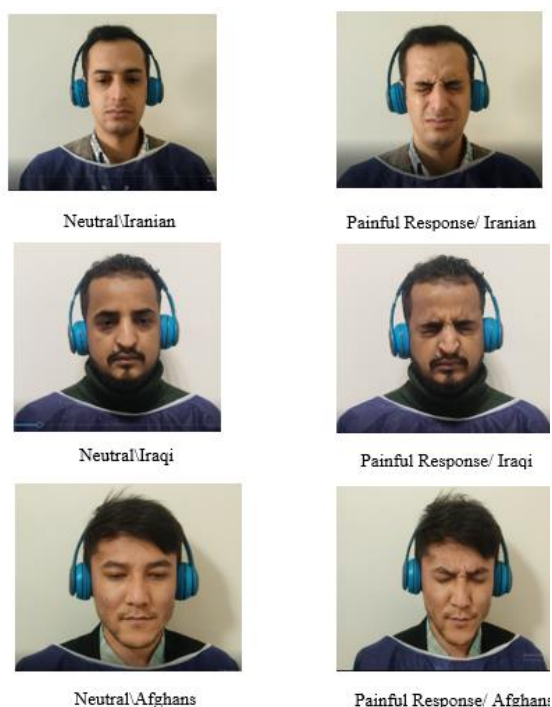


Figure 1. Sample frames of facial expressions shifting from neutral to pain due to an aversive sound

genuine intense pain expression were selected for an fMRI test. A group of 10 people rated these clips on a scale of 1 to 5. There were 16 video subjects (8 males) from each ethnicity.

2.4. Functional MRI Scanning

Before their fMRI scans, participants were told to watch video clips of patients with neurological hearing issues undergoing painful sound therapy. Before each video clip, there were written instructions that described the patients' diagnoses, which were either acquired during their life or caused by hereditary factors due to their father's involvement in wars. Participants conducted a trial before the scan to familiarize themselves with the button box.

We conducted a study using a 3x2 factorial design, which looked at the origin (Iranian/Iraqi/Afghan) and type of disease (hereditary/acquired) as factors. The stimuli were presented in a blocked event-related mode, with fixation images shown before each video clip. The patients' nationalities were indicated in the instructions. Participants watched 8-second video clips of a male and female with neutral expressions for 0.5 seconds, followed by painful expressions for 7.5 seconds. They used a 1 to 4 scale to rate the intensity of the perceived pain.

3. Results

We conducted an MRI at Iran's National Brain Mapping Lab to study empathy-related responses. We used a 3-T Siemens Sonata scanner for 2 fMRI runs with 48 video clips. We collected behavioral data and created visual content using Psychopy2021 software. Our team processed the images using the SPM test in Mathworks Matlab R2022a software. Participants received random and equal blocks with six positions. Each round had two video clips (male and female) for each condition, repeated four times with a two-minute rest in between.

The control group showed higher activity in the corpus callosum when observing Iranian's pain (heredity condition). ($p < 0.001$) (Figure 2). CC is a crucial area for social cognition, which includes empathy as an important capacity. Recent studies have shown that damage to this area due to brain trauma can impair social cognition. Additionally, microstructural

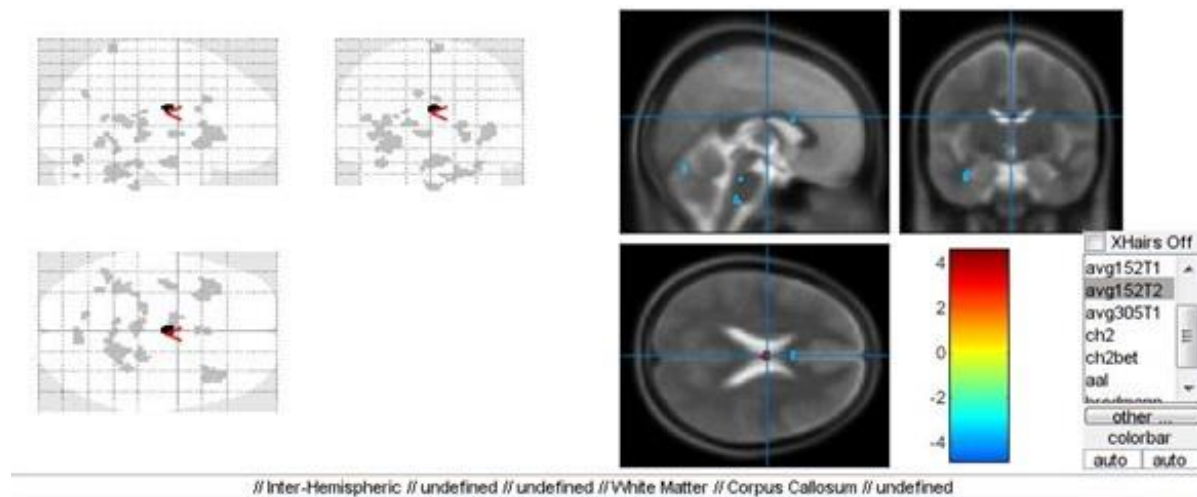


Figure 1. Between Group Analysis/ CC activated in Control Group. Contrast (Irani Heredity>Iraqi Heredity) $p < 0.001$

studies have revealed that white matter connectivity, particularly through CC, can predict emotional empathy ability. Evidence suggests that the corpus callosum plays a significant role in empathy [20-22]. This finding supports the initial assumption of the study that the main group has a lower empathy capacity than the control group.

The main group had higher insula activity when observing pain in Iranian subjects (heredity condition). ($p < 0.001$) The insula is involved in empathic responses to pain and emotions such as disgust, fear, anxiety, and happiness. The right anterior insula is linked to affective-perceptual empathy, while the left is linked to affective-cognitive and cognitive-evaluative empathy. Stimulation of the left insula can affect the ability to recognize emotions,

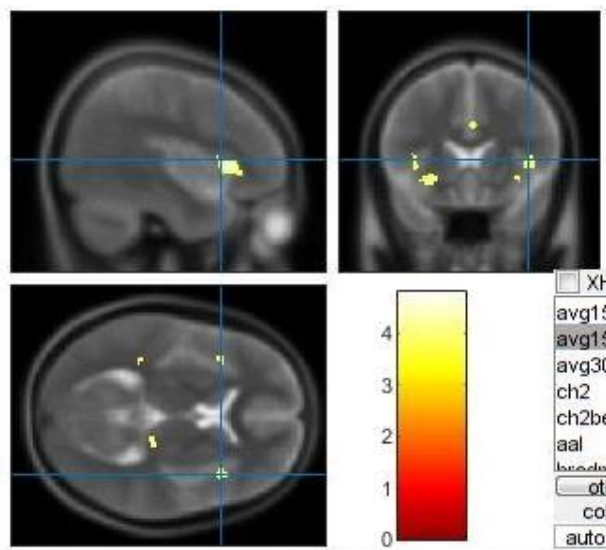


Figure 3. Insula activated in the main group. Contrast (Iranian heredity>Iraqi Heredity), $p < 0.001$

particularly disgust. The insula is also implicated in biased empathy, with increased activity in the bilateral anterior insula associated with a tendency to harm stereotyped out-groups. The left insula is affected in cases of national-regional group membership and in-group bias [23-26] (Figure 3).

The Control group had higher activity in limbic and parahippocampal fusiform when observing pain in Iraqi subjects (Figure 4).

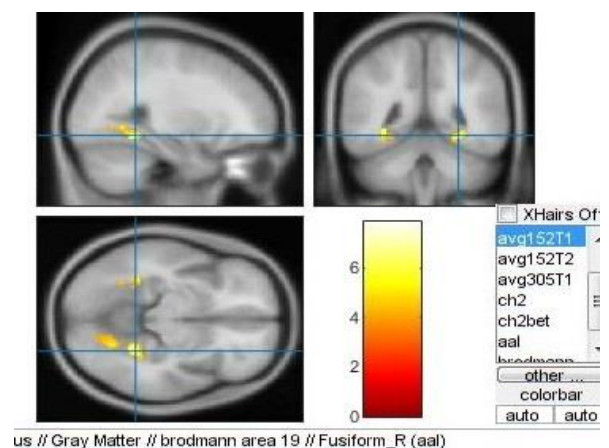


Figure 2. Limbic area activated in the control group. Contrast (Iraqi heredity>Iranian Heredity), $p < 0.001$

When viewing the facial pain of an Iraqi with a hereditary condition, the main group displayed greater activity in the Occipital Lobe and Lingual Gyrus ($p \text{ Value} < 0.001$). The occipital lobe is responsible for processing empathy triggered by pain from visual stimuli. An increase in activity in this area suggests that empathy processing is occurring at an early stage. However, it is worth noting that the

activity of this area is solely influenced by the type of stimulus utilized during the experiment (Figure 5).

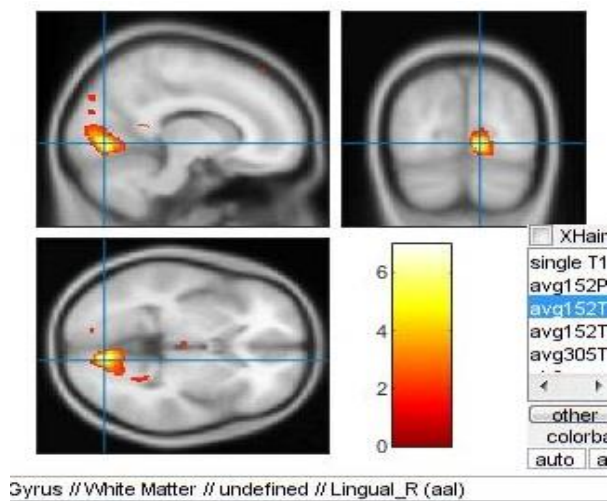


Figure 5. Occipital Lobe and Lingual Gyrus activated in the control group. Contrast (Iraqi heredity>Iranian Heredity), $p < 0.001$

4. Conclusion

Our study aimed to investigate whether children of Iran-Iraq war survivors, who have experienced war trauma, exhibit reduced empathy toward Iraqis. The results showed a significant decrease in empathy among the offspring of war survivors with a family history of trauma. The control group exhibited higher activity in the corpus callosum when observing Iranian's pain, indicating the region's importance in social cognition and empathy. On the other hand, the main group showed higher insula activity when watching Iranian pain, which is involved in empathic responses to pain and in-group favoritism. These findings suggest that the main group may have a lower empathy capacity than the control group. Our fMRI study offers valuable insights into the complex neurobiological mechanisms underlying the intergenerational transmission of war trauma. It may have important implications for future research in the interdisciplinary field of peace and neuroscience. It highlights the need to address the long-term impacts of war trauma on future generations and the importance of effective interventions to promote empathy and reduce in-group favoritism among individuals with war-related trauma family backgrounds.

Acknowledgments

This research has been supported by Iran Cognitive Sciences and Technologies Council based on the project with code number 9327. The authors would like to acknowledge National Brain Mapping Laboratory (NBML), Tehran, Iran, for providing data acquisition and analysis services for this research work.

References

- 1- Levy, J., Goldstein, A., & Feldman, R. "The neural development of empathy is sensitive to caregiving and early trauma." *Nature Communications*, 10(1), (2019).
- 2- Mazza, M., Tempesta, D., Pino, M. C., Nigri, A., Catalucci, A., Guadagni, V., ... & Ferrara, M. "Neural activity related to cognitive and emotional empathy in post-traumatic stress disorder." *Behavioural brain research*, 282, 37-45, (2015).
- 3- Eidelman-Rothman, M., Goldstein, A., Weisman, O., Schneiderman, I., Zagoory-Sharon, O., Decety, J., & Feldman, R. "Prior exposure to extreme pain alters neural response to pain in others." *Cognitive, affective, & behavioral Neuroscience*, 16, 662-671, (2016).
- 4- Driscoll, D. M., Dal Monte, O., Solomon, J., Krueger, F., & Grafman, J. "Empathic deficits in combat veterans with traumatic brain injury: a voxel-based lesion-symptom mapping study." *Cognitive and behavioral neurology*, 25(4), 160-166, (2012).
- 5- Beckham, J. C., Braxton, L. C., Kudler, H. S., Feldman, M. E., Lytle, B. L., & Palmer, S. "Minnesota Multiphasic Personality Inventory profiles of Vietnam combat veterans with posttraumatic stress disorder and their children." *Journal of Clinical Psychology*, 53(8), 847-852, (1997).
- 6- Yehuda, R. "Parental PTSD as a risk factor for PTSD. In R. Yehuda (Ed.), Risk factors for posttraumatic stress disorder" (pp. 93-123). *American psychiatric association*, (1999).
- 7- Yehuda, R., Halligan, S. L., & Bierer, L. M. "Relationship of parental trauma exposure and PTSD to PTSD, depressive and anxiety disorders in offspring." *Journal of Psychiatric Research*, 35(5), 261-270, (2001). [https://doi.org/10.1016/S0022-3956\(01\)00032-2](https://doi.org/10.1016/S0022-3956(01)00032-2)
- 8- Kellerman, N. Transgenerational effects of the Holocaust: *The Israeli research perspective*. In Z. Solomon & J. Chaitin (Eds.), *Childhood in the shadow of the holocaust—Survived children and second-generation* (pp. 286-303). Tel Aviv, Israel: Hakibbutz Hameuchad, (2007).

- 9- Banneyer, K. N., Koenig, S. A., Wang, L. A., & Stark, K. D. "A review of the effects of parental PTSD: A focus on military children. Couple and Family Psychology: *Research and Practice*, 6(4), 274, (2017).
- 10- Kellermann, N. P. "Epigenetic transmission of holocaust trauma: can nightmares be inherited." *The Israel Journal of Psychiatry and Related Sciences*, 50(1), 33-39, (2013).
- 11- Perroud, N., Paoloni-Giacobino, A., Prada, P., Olié, E., Salzman, A., Nicastro, R., ... & Malafosse, A. "Increased methylation of glucocorticoid receptor gene (NR3C1) in adults with a history of childhood maltreatment: a link with the severity and type of trauma." *Translational psychiatry*, 1(12), e59-e59, (2011).
- 12- Chan, J. C., Nugent, B. M., & Bale, T. L. "Parental advisory: maternal and paternal stress can impact offspring neurodevelopment." *Biological Psychiatry*, 83(10), 886-894, (2018).
- 13- Yehuda, R., & Lehrner, A. "Intergenerational transmission of trauma effects: putative role of epigenetic mechanisms." *World psychiatry*, 17(3), 243-257, (2018).
- 14- Davis, M. H. "Measuring individual differences in empathy: Evidence for a multidimensional approach." *Journal of personality and Social psychology*, 44, 113-126, (1983).
- 15- Bernstein, D. P., Stein, J. A., Newcomb, M. D., Walker, E., Pogge, D., Ahluvalia, T., & Zule, W. Development and validation of a brief screening version of the Childhood Trauma Questionnaire. *Child Abuse and Neglect*, 27 (2), 169-190, (2003).
- 16- Yehuda R, Labinsky E, Tischler L, Brand SR, Lavin Y, Blair W, et al.: "Are adult offspring reliable informants about parental PTSD? A validation study." *Ann N Y Acad Sci*, 1071:484-487, (2006).
- 17- Lamm, C., Nusbaum, H. C., Meltzoff, A. N., & Decety, J. "What are you feeling? Using functional magnetic resonance imaging to assess the modulation of sensory and affective responses during empathy for pain." *PloS one*, 2(12), e1292, (2007).
- 18- Contreras-Huerta, L. S., Baker, K. S., Reynolds, K. J., Batalha, L., & Cunnington, R. "Racial bias in neural empathic responses to pain." *PloS one*, 8(12), e84001, (2013).
- 19- Craig, K. D., Prkachin, K. M., & Grunau, R. V. E. "The facial expression of pain." In D. C. Turk & R. Melzack (Eds.), *Handbook of pain assessment* (2nd ed., pp. 153-169). New York: Guilford, (2001).
- 20- Aboitiz, F., & Montiel, J. "One hundred million years of interhemispheric communication: the history of the corpus callosum." *Brazilian Journal of Medical and Biological Research*, 36, 409-420, (2003).
- 21- Bastos Jr, M. A. V., Bastos, P. R. H. O., Foschaches Filho, G. B., Conde, R. B., Ozaki, J. G. O., Portella, R. B., ... & Lucchetti, G. "Corpus callosum size, hypnotic susceptibility and empathy in women with alleged mediumship: a controlled study." *EXPLORE*, 18(2), 217-225, (2022).
- 22- McDonald, S., Rushby, J. A., Dalton, K. I., Allen, S. K., & Parks, N. "The role of abnormalities in the corpus callosum in social cognition deficits after Traumatic Brain Injury." *Social neuroscience*, 13(4), 471-479, (2018).
- 23- Pugnaghi M, Meletti S, Castana L, et al. "Features of somatosensory manifestations induced by intracranial electrical stimulations of the human insula." *Clin neurophysiol.*;122:2049-2058, (2011).
- 24- Cikara, M., Bruneau, E., Van Bavel, J. J., & Saxe, R. "Their pain gives us pleasure: How intergroup dynamics shape empathic failures and counter-empathic responses." *Journal of Experimental Social Psychology*, 55, 110-125, (2014).
- 25- Uddin, L. Q., Nomi, J. S., Hébert-Seropian, B., Ghaziri, J., & Boucher, O. "Structure and function of the human insula." *Journal of clinical neurophysiology: official publication of the American Electroencephalographic Society*, 34(4), 300, (2017).
- 26- Saarinen, A., Jääskeläinen, I. P., Harjunen, V., Keltikangas-Järvinen, L., Jasinskaja-Lahti, I., & Ravaja, N. "Neural basis of in-group bias and prejudices: A systematic meta-analysis." *Neuroscience & biobehavioral reviews*, 131, 1214-1227, (2021).



Impact of Diffusion Tensor Field Smoothing with Log-Cholesky Metric on Noise Reduction

Somayeh Jaberi^{1*} , Amin Ghodousian¹, Babak Ardekani²

¹College of Engineering, Faculty of Engineering Science, Algorithms and Computation Group, University of Tehran, Tehran, Iran

²Center for Advanced Brain Imaging and Neuromodulation, The Nathan S. Kline Institute for Psychiatric Research, Orangeburg, New York USA

*Corresponding Author: Somayeh Jaberi

Email: sjabari@ut.ac.ir

Abstract

Diffusion Tensor Imaging (DTI) is a noise-sensitive method, where a low Signal-to-Noise Ratio (SNR) results in significant errors in the estimated tensor field. Post-reconstruction tensor field smoothing is a simple and effective solution for alleviating this problem. Diffusion tensors can be represented by Symmetric Positive-Definite (SPD) matrices which can be viewed as a Riemannian manifold after defining a suitable metric on the space of SPD matrices. The Log-Cholesky metric is a recently developed concept with several advantages over previously defined metrics, e.g., Frobenius, Log-Euclidean, and affine-invariant metrics. In this work, we implemented a smoothing method based on the Log-Cholesky metric and show its effectiveness as a simple solution to filtering noisy diffusion tensor fields.

Keywords: Tensor Field Smoothing; Diffusion Tensor Imaging; Log-Cholesky Metric; Riemannian Geometry.

1. Introduction

DTI has become the method of choice in Magnetic Resonance Imaging (MRI) for imaging the brain white matter. In DTI, for each voxel of the brain, a diffusion tensor is estimated using a series of Diffusion Weighted Images (DWI). Low SNR in DWI may result in significant errors in the estimated tensors which adversely impact subsequent analyses, for example, in white matter tractography. Therefore, regularization of the estimated tensor field is necessary to reduce the impact of noise.

The state-of-the-art noise reduction methods apply the regularization during tensor reconstruction. However, these methods are often complex and computationally inefficient. Spatial smoothing of the tensor field post-reconstruction presents a practical alternative. Smoothing basically amounts to spatial averaging of the reconstructed noisy tensors. However, the averaging needs to be performed in the SPD space using Riemannian geometry based on a selected Riemannian metric. Previously utilized metrics for this purpose are the Frobenius, the Log-Euclidean, and the affine-invariant (Fisher). The Log-Cholesky metric [1] has been introduced recently as an alternative with several advantages, e.g., computational efficiency, non-swelling effect, a closed-form average.

2. Materials and Methods

In DTI tensors are estimated by fitting the Stejskal-Tanner model [2], $S_i = S_0(-bg_i^t D g_i)$, to the DWI data, S_i , where D is a 3×3 SPD matrix to be estimated at each voxel.

Usually, a least squares method is used for tensor estimate, such as linear (LLS) or Non-linear Least Squares (NLS) [3], or Iterative Re-Weighted (IRWLS) [4]. We implemented these methods while imposing positivity constraints [3]. Following tensor field estimation, we use the Log-Cholesky metric in the context of Riemannian geometry to spatially smooth the tensor field.

Briefly, the Cholesky decomposition establishes a diffeomorphism between the space of SPD matrices and the space of lower triangular matrices with positive diagonal elements (\mathcal{L}^+). In the present paper,

we perform the smoothing in \mathcal{L}^+ . Specifically, to average a set of adjacent SPD matrices, D_1, D_2, \dots, D_n , we first compute their corresponding elements in \mathcal{L}^+ , L_1, L_2, \dots, L_n , and then average them as follows (Equation 1):

$$L_{ave} = \frac{1}{n} \sum_{i=1}^n [L_i] + \exp \left(\frac{1}{n} \sum_{i=1}^n \log \mathbb{D}(L_i) \right) \quad (1)$$

where $[L_i]$ is the strictly lower triangular part and $\mathbb{D}(L_i)$ is the diagonal part of L_i . The average D_{ave} is finally given by (Equation 2):

$$D_{ave} = L_{ave} L_{ave}^T \quad (2)$$

3. Results and Discussion

IRWLS with and without post-reconstruction smoothing was implemented in Python. We used simulated DWI data to compare IRWLS with and without smoothing. The simulated DWI was created by ExploreDTI [5] with 32 directions. Figure 1 shows the estimated tensor fields using IRWLS alone and using IRWLS followed by Log-Cholesky post-reconstruction smoothing (SNR=15). Figure 2 compares the error distributions (i.e., distances between the simulated and estimated tensors) between IRWLS and IRWLS+smoothing methods.

Qualitatively, Figure 1 shows that post-reconstruction Log-Cholesky smoothing clearly improves the estimated tensor field. Noise is reduced while tensor orientation and boundaries are well preserved.

Quantitatively, Figure 2 shows that smoothing clearly shifts the distribution of errors to the right when smoothing is applied

4. Conclusion

Post-reconstruction smoothing using the Log-Cholesky method clearly improves DTI estimation. This can be a simple and effective method for noise reduction which can be applied as an independent processing step in DTI analysis, as an alternative to complex methods that implement regularization during DTI reconstruction.

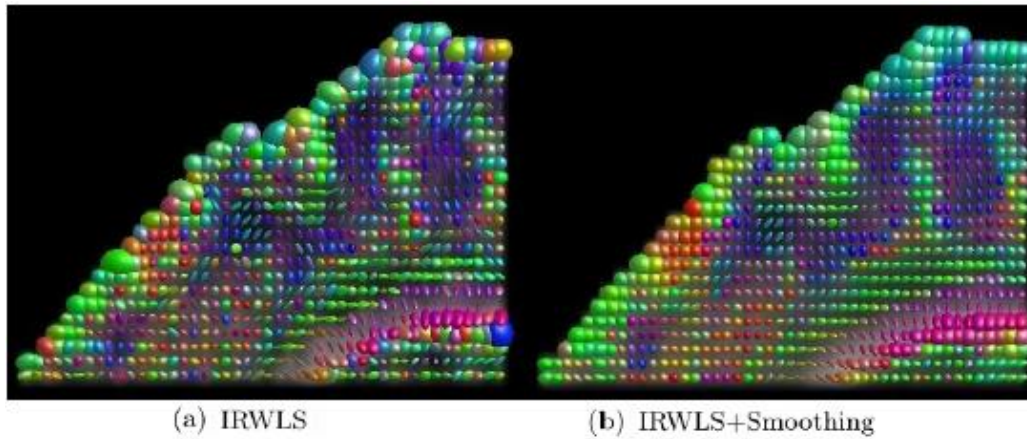


Figure 1. Estimated tensor fields. (a) using IRWLS, (b) using IRWLS+Smoothing

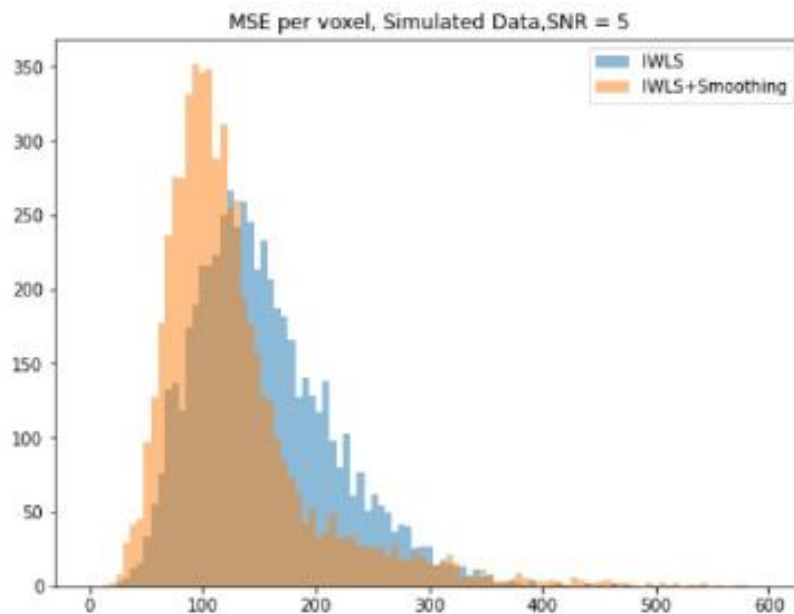



Figure 2. Comparison of error distributions between IRWLS and IRWLS+Smoothing methods

References

- 1- Zhenhua Lin, "Riemannian Geometry of Symmetric Positive Definite Matrices via Cholesky Decomposition," *SIAM Journal on Matrix Analysis and Applications*, vol. 4, no. 40, pp. 1353-1370, 2019.
- 2- E. O. Stejskal and J. E. Tanner, "Spin Diffusion Measurements: Spin Echoes in the Presence of a Time Dependent Field Gradient," *THE JOURNAL OF CHEMICAL PHYSICS*, vol. 42, pp. 288-292, August 1965.
- 3- C. G. Koay, L.-C. Chang, J. D. Carew, C. Pierpaoli, and P. J. Basser, "A unifying theoretical and algorithmic framework for least squares methods of estimation in diffusion tensor imaging," *Journal of Magnetic Resonance*, vol. 182, pp. 115-125, 2006.
- 4- Q. Collier, J. Veraart, B. Jeurissen, A. J. Dekker, and J. Sijbers, "Iterative reweighted linear least squares for accurate, fast, and robust estimation of diffusion magnetic resonance parameters," *Magnetic Resonance in Medicine*, vol. 73, p. 2174-2184, 2015.
- 5- A. Leemans, B. Jeurissen, J. Sijbers, and D. K. Jones, "ExplorDti: a graphical toolbox for processing, analyzing, and visualizing diffusion mr data.," *17th Annual Meeting of Intl Soc Mag Reson Med*, 2009.



Deep Multimodal Active Contour for Automatic Ischemic Stroke Lesion Segmentation

Asieh Khosravanian ^{1*} , Ali Rezaei ¹, Kamran Kazemi ¹, Ardalan Aarabi ²

¹Department of Electrical and Electronics Engineering, Shiraz University of Technology, Shiraz, Iran

²Faculty of Medicine, University of Picardy Jules Verne, Amiens, France

*Corresponding Author: Asieh Khosravanian
Email: khosravanian.a@gmail.com

Abstract

Ischemic stroke lesion segmentation in Magnetic Resonance Images (MRIs) is a challenging task due to lesion type, shape, and size variations in the brain. Also, MRIs suffer from intensity inhomogeneity and different types of noises. Lesion segmentation is a manual task for clinicians which is error-prone and very time-consuming. This paper aims to present an automatic segmentation for Ischemic stroke lesions in MRIs.

The proposed method is a new active contour model based on morphology and fuzzy kernel clustering with a combination of modified U-Net for initial contour selection. In this way, a fully automatic stroke lesion segmentation is obtained.

Experiments are conducted on ISLES 2015 dataset. We use T2 and Flair modalities as a vector-valued approach for multimodal segmentation. Results show that our proposed method can segment stroke lesions with proper accuracy. Dice, Jaccard, Sensitivity, and Specificity for automatic lesion segmentation against ground truth are 0.9652 ± 0.0316 , 0.9344 ± 0.0561 , 0.9903 ± 0.0033 and 0.9903 ± 0.0033 respectively.

Our multimodal proposed method shows satisfactory results for Ischemic lesion segmentation due to fuzzy clustering and morphological approach. Moreover, our method is not sensitive to initialization thanks to the proposed modified U-Net. Also, our method is capable to segment images with intensity inhomogeneity.

Keywords: Active Contour; Deep Learning; Ischemic Stroke Lesion Segmentation; Kernel Induced Clustering; Morphology.

1. Introduction

Brain stroke is the second leading cause of death in the world [1]. Brain stroke is a series of brain tissue necrosis symptoms caused by rupture or blockage of intracranial blood vessels [2]. Lesion segmentation from MRI means marking each voxel as a lesion or non-lesion. Automatic lesion segmentation is an important task for the diagnosis of ischemic stroke because manual lesion segmentation by physicians is tedious and time-consuming. However, automatic segmentation is challenging since the lesions have a large variation of location, irregular boundaries and shape, and appearance at different times in the brain [3]. In recent years, there has been growing interest in automatic segmentation of brain lesions such as tumors and stroke [4-6]. In this paper, we present a new active contour model based on morphological fuzzy clustering and deep learning for automatic stroke lesion segmentation.

2. Materials and Methods

The proposed method consists of two major parts. In the first part, we proposed modified attention U-Net and in the second part, we introduced a new region-based active contour for segmentation.

2.1. Proposed Modified Attention U-Net

The proposed architecture includes an encoder, decoder, and modified attention blocks. The encoder

and decoder blocks have five layers including the max pooling layers. To reduce the number of trainable parameters, the DWS-ResBlock3d layer is designed and used in the encoder.

2.2. Proposed Morphological Kernel Fuzzy

The lesion segmentation was performed using the kernel fuzzy active contour model proposed by Khosravianian *et al.* [7].

$$\begin{aligned}
 F_K(R_1, R_2, u, v, B) &= \int_{R_1} u_1^p(\vec{x}) J_K(I(\vec{x}), b(\vec{x})v_1) M_1(\varphi) d\vec{x} \\
 &+ \int_{R_2} u_2^p(\vec{x}) J_K(I(\vec{x}), b(\vec{x})v_2) M_2(\varphi) d\vec{x} \\
 &+ vL(\varphi) + \mu R_p(\varphi)
 \end{aligned} \tag{1}$$

Where the image intensity $I(\vec{x})$ corresponding to the object domain Ω_i is approximated by a local mean of $b(\vec{x})c_i$. The $b(\vec{x})$ is a smooth and spatially varying function that models the intensity non-uniformity. The u_i^p indicates the membership function in fuzzy clustering. The characteristic functions of regions are $M_1(\varphi) = H(\varphi)$ and $M_2(\varphi) = 1 - H(\varphi)$. The $L(\varphi)$ and $R_p(\varphi)$ are an arc term and a distance regularization term, respectively.

We used morphological operators for contour evolution [8] as a novelty in this paper instead of the traditional minimization method in the active contours. In this regard, the energy function is minimized by the following three steps:

Step 1:

$$\varphi^{m+1/3}(x) = \begin{cases} \text{Dilate}(\varphi^m(x)) & v > 0 \\ \text{Erode}(\varphi^m(x)) & v < 0 \\ \varphi^m(x) & \text{otherwise} \end{cases} \tag{2}$$

Step 2:

$$\varphi^{m+2/3}(x) = \begin{cases} 1 & |\nabla \varphi^{m+1/3}| \cdot \left(\int_{R_1} u_1^p(\vec{x}) J_K(I(\vec{x}), B(\vec{x})v_1) M_1(\varphi) d\vec{x} + \int_{R_2} u_2^p(\vec{x}) J_K(I(\vec{x}), B(\vec{x})v_2) M_2(\varphi) d\vec{x} \right) < 0 \\ 0 & |\nabla \varphi^{m+1/3}| \cdot \left(\int_{R_1} u_1^p(\vec{x}) J_K(I(\vec{x}), B(\vec{x})v_1) M_1(\varphi) d\vec{x} + \int_{R_2} u_2^p(\vec{x}) J_K(I(\vec{x}), B(\vec{x})v_2) M_2(\varphi) d\vec{x} \right) > 0 \\ \varphi^{m+1/3} & \text{otherwise} \end{cases} \tag{3}$$

Step 3:

$$\varphi^{m+1}(x) = \text{opening}(\text{closing}(\mathcal{C}(\varphi^{m+2/3}(x)))) \quad \mu \text{ Times} \tag{4}$$

3. Results

To evaluate the performance of the proposed method, we used the T2 and Flair modalities from ISLES 2015 simultaneously. The proposed modified attention U-Net was trained on 70% of three-dimensional MRIs. To evaluate the efficiency of the proposed morphological kernel fuzzy level set model, 10 cases were selected randomly. The proposed U-Net segmentation results are used as an initial contour in the proposed multimodal active contour model. Results confirm that multimodal active contour capable to improve the results of the proposed modified U-Net.

Figure 1 shows the segmentation results by the proposed method. The quantitative results of the proposed method are shown in Table 1.

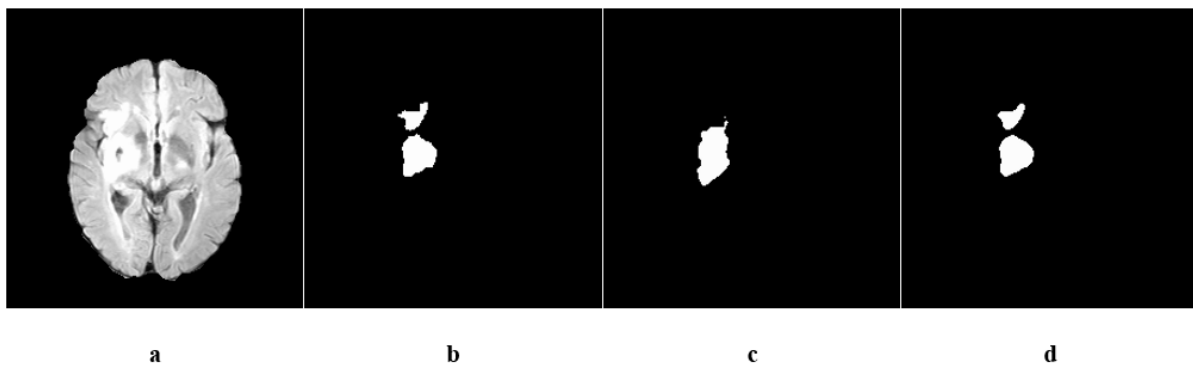


Figure 1. Proposed method results a: Original Image (Flair modality), b: Reference mask c: Proposed U-Net segmentation result, d: Proposed multimodal segmentation result

Table 1. Quantitative results (mean \pm std)

Method	Dice	Jaccard	Sensitivity	Specificity
Proposed modified attention U-Net	0.8215 \pm 0.1583	0.7181 \pm 0.1768	0.8071 \pm 0.2049	0.9979 \pm 0.0024
Proposed active contour	0.9652 \pm 0.0316	0.9344 \pm 0.0561	0.9903 \pm 0.0033	0.9903 \pm 0.0033

Acknowledgment

This work is based upon funded by Iran National Science Foundation (INSF) under project No. 4002296.

4. Conclusion

In this paper, we proposed a deep multimodal active contour method that automatically segmented stroke lesions from 3D MRIs with high accuracies. The proposed method used a modified attention U-Net for initial contour selection. The results show that our method can improve the U-Net results in stroke lesion segmentation.

References

- 1- Kamalakannan, S., et al., "Incidence & prevalence of stroke in India: A systematic review." *The Indian journal of medical research*, 146(2): p. 175, (2017).
- 2- Wu, Z., et al., "Multi-scale long-range interactive and regional attention network for stroke lesion segmentation." *Computers and Electrical Engineering*, 103: p. 108345, (2022).

- 3- Gonzalez, R., *et al.*, "Acute ischemic stroke. Imaging and intervention| Springer-Verlag, Berlin Heidelberg 2006.", *Elsevier Masson*, (2006).
- 4- Chavva, I.R., *et al.*, "Deep learning applications for acute stroke management." *Annals of Neurology*, 92(4): p. 574-587, (2022).
- 5- Khosravanian, A., *et al.*, "Enhancing level set brain tumor segmentation using fuzzy shape prior information and deep learning." *International Journal of Imaging Systems and Technology*, 33(1): p. 323-339, (2023).
- 6- Ghaffari, M., A. Sowmya, and R. Oliver, "Automated brain tumor segmentation using multimodal brain scans: a survey based on models submitted to the BraTS 2012–2018 challenges." *IEEE reviews in biomedical engineering*, 13: p. 156-168, (2019).
- 7- Khosravanian, A., *et al.*, "Level set method for automated 3D brain tumor segmentation using symmetry analysis and kernel induced fuzzy clustering." *Multimedia Tools and Applications*, 81(15): p. 21719-21740, (2022).
- 8- Marquez-Neila, P., L. Baumela, and L. Alvarez, "A morphological approach to curvature-based evolution of curves and surfaces." *IEEE Transactions on Pattern Analysis and Machine Intelligence*, 36(1): p. 2-17, (2013).



High-Efficiency Graph Measures in Discriminating Schizophrenia Patients from Healthy Controls Using Structural and Functional Connectivity

Mahya Naghipoor Alamdari¹, Jafar Zamani², Farzaneh Keyvanfard³, Abbas Nassiraei Moghadam^{1,3*} 

¹Department of Biomedical Engineering, Amirkabir University of Technology, Tehran, Iran

²School of Electrical Engineering, Iran University of Science and Technology, Tehran, Iran

³School of Cognitive Sciences, Institute for Research in Fundamental Sciences (IPM), Tehran, Iran

*Corresponding Author: Abbas Nassiraei Moghadam

Email: nasiraei@aut.ac.ir

Abstract

The human brain is a complex network characterized by structural and functional connections within and between regions. It is proven that in some brain diseases (such as schizophrenia), these connections are disrupted. Graph theory is a suitable tool to analyze brain network disruptions. The data analyzed in this study include the functional and structural connections of 27 schizophrenic patients and 27 healthy controls. By means of Independent Component Analysis (ICA) and joint ICA (jICA) algorithms, the brain network is divided into 10 sub-networks, in which structural connections play an important role. We look for graph parameters that distinguish patients from healthy people. We observed that the local parameters of joint subnetwork #3 such as clustering efficiency, strength, and local efficiency can be used to distinguish patients from controls. The global parameters in joint subnetwork #1, such as characteristic path length, radius, diameter, and max modularity have the same effect. To investigate nervous system disorders such as schizophrenia it is better to analyze the joint sub-networks of the brain than the whole brain.

Keywords: Schizophrenia; Independent Component Analysis; Subnetworks; Functional Connectivity; Graph Theory.

1. Introduction

The brain consists of several complex networks that reveal its structural and functional connections [1]. This approach provides a higher-level description of complex human behaviors and psychological disorders [2, 3]. In recent studies, instead of the whole brain, we may consider its subnetworks, which provide suitable concepts for studying neuroscience and analyzing the connectivity of the brain [4]. In this study, a network-level blind analysis is used to decompose brain connectivity into subnetworks based on Independent Component Analysis (ICA) [5]. As a result, 10 joint networks have been constructed from functional and structural connections of 27 persons with schizophrenia and 27 healthy individuals. The main features of schizophrenia include cognitive dysfunction associated with poor occupational and social performance [6]. This psychotic disorder such as schizophrenia may be caused by changes in the dynamics of connections between the brain segments. The disorders known in schizophrenia can be well studied with imaging techniques, including fMRI and DTI. The use of the joint algorithm on multimodal data has led to the discovery of the relationship between the structure and the function of the brain. Such analysis examines the information from two or more modalities together which helps in detecting their mutual counterparts and extracting more comprehensive information compared to a single modality [7, 8]. In this study, graph theory has been exploited to calculate the parameters of both structural and functional subnetworks jointly. Diagnosis and estimation of topology changes using various graph parameters can provide a proper understanding of the pathophysiological mechanism of this disease. Thus, changes in brain connections can be detected using graph parameters and subnetworks that are most sensitive in schizophrenia.

2. Materials and Methods

The data used in this study are the structural and functional connectivity matrices of 27 people living with schizophrenia and 27 healthy subjects. The Lausanne atlas was used for brain parcellation [9]. PCA is used for dimensionality reduction. Then two algorithms ICA and jICA are used to divide the brain

connectivity network into 10 sub-networks. ICA considers only the functional connectivity, while jICA takes also into account the structural connectivity. After determining the location of each subnetwork, the differences between the two groups were analyzed using graph theory. Graph parameters studied in this article include betweenness, clustering coefficient, modularity maximization, diffusion, strength, local and global efficiency, radius, diameter, characteristic path length, modularity optimum, and node eccentricity, which were examined by statistical analysis. The algorithms for constructing subnetworks and calculation of the graph parameters are implemented using MATLAB 2021b and Brain Connectivity Toolbox (BCT), a powerful MATLAB toolbox for graph analysis. The goal is to see if graph parameters of certain subnetworks can discriminate between schizophrenic and healthy individuals.

3. Results

Figure 1 shows the similarities between the jICA and ICA subnetworks. The similarities between these two types of subnetworks are calculated in each of their 10 subnetworks. The highest similarities have been observed between jICA subnetworks #1 to #10 to ICA subnetworks #8, #5, #1, #1, #2, #4, #7, #7, #5, and #5 respectively. The differences between the 2 types of subnetworks are due to the presence of structural information in the analysis. Consequently, joint analysis offers the possibility of extracting more comprehensive information than other methods because it examines the information from two or more modalities together and it is possible to detect the equivalence between them. Also, structural connectivity leads to different subnetworks compared to other methods. In other words, the relationship between brain structure and function is not necessarily one-to-one, and it appears that connections are structural, they have the ability to control functional connections indirectly and remotely [10-13].

Using a t-test with a p-value of less than 0.05, the significant global graph parameters of jICA subnetworks are as follows: the radius in the subnetworks #1 and #3, the maximum modularity in subnetworks #1, #4, and #9, the characteristic path length in subnetwork #1, the diameter in subnetworks #1 and #3, and the global efficiency in subnetwork #1,

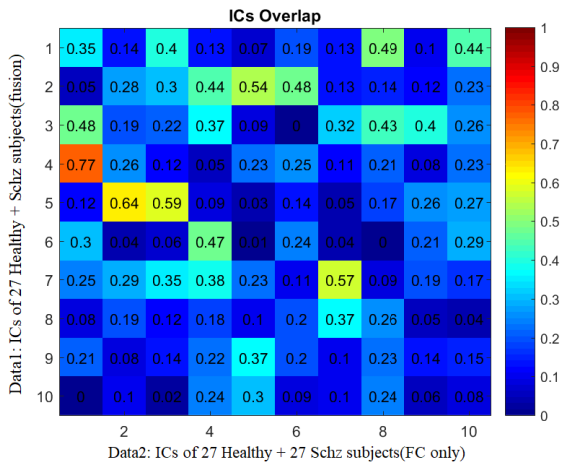


Figure 1. Similarities of jICA (functional and structural) subnetworks with ICA (functional-only) subnetworks

which can be distinguished from healthy people and schizophrenics by studying these parameters in specific subnetworks. It is notable that most of the global parameters are significant in sub-network #1 which includes the default mode network (DMN) and the limbic areas in the brain. For jICA subnetworks, the significant local parameters are as follows: strength in subnetworks #3 and #5 and cluster coefficient in subnetworks #3 and #7, eccentricity in subnetwork #10 and #2, and local efficiency in subnetworks #3, #5, and #7, which distinguish patients from healthy individuals. In this type of local parameters, subnetwork #3 can be used to diagnose

schizophrenia by examining the neurological disorders of this subnetwork, which mainly includes the visual and sensorimotor areas. The subnetworks created using only functional connectivity contain significant graph parameters: Radius in subnetworks #10, #1, #7, and #8; characteristic path length in subnetworks #5, #7, and #9; maximum modularity in subnetwork #1; global efficiency in subnetworks #5, #7, and 9; diffusion in subnetwork #8; and diameter in subnetwork #1 distinguish healthy and schizophrenic patients. Similarly, strength in subnetworks #5, #7, and #9, local efficiency in subnetworks #5, #7, and #9, eccentricity in subnetwork #1, and clustering coefficient in subnetworks #5, #7, and #9 distinguish patients from control subjects. Consequently, neurological disorders in schizophrenia patients can be diagnosed by examining subnetworks #5 (which includes ventral attention and area SM at rest) and #7, which includes area SM (which are only the result of functional connections, for many parameters. Table 1 shows the details of the statistical results. In contrast, when the clustering coefficient, radius, and characteristic path length parameters were examined for the whole brain, a significant difference was found between the healthy subjects and the patients. Thus, if the subnetworks were not used and only the state of the whole brain was considered, more detailed information about the disorders occurring in schizophrenia and their exact localization would not be obtained.

Table 1. Details of the statistical results. significant parameters in just and joint functions

Function	Subnetwork	Parameter	P-value	CTRL Mean & std	SZ Mean & std
just function	#7	Clustering Coefficient	0.0010	0.0808 ± 0.0169	0.0687 ± 0.0133
		Strength	0.0030	9.9264 ± 1.6259	8.8630 ± 1.3269
		Local Efficiency	0.0032	0.1486 ± 0.0276	0.1311 ± 0.231
		Radius	0.0050	6.5527 ± 0.5724	6.9812 ± 0.5899
		Global Efficiency	0.0109	0.2278 ± 0.0249	0.2133 ± 0.0210
		Eccentricity	0.0305	8.1626 ± 0.7853	8.5957 ± 0.7354
		Characteristic path length	0.0395	4.9885 ± 0.5167	5.2596 ± 0.4704
		Clustering Coefficient	0.0089	0.0930 ± 0.0172	0.0806 ± 0.0178
		Local Efficiency	0.0147	0.1640 ± 0.0276	0.1458 ± 0.0283
		Strength	0.0154	9.3982 ± 1.3596	8.4650 ± 1.4123
joint function	#5	Global Efficiency	0.0195	0.2288 ± 0.0231	0.2142 ± 0.0227
		Characteristic path length	0.0378	5.0278 ± 0.5156	5.3170 ± 0.5082
		Radius	0.03632	5.6983 ± 0.5456	6.1127 ± 0.5229
	#3	Strength	0.04471	17.2229 ± 3.5778	15.5285 ± 2.3429
		Local Efficiency	0.04858	0.1794 ± 0.0427	0.1601 ± 0.0281
		Clustering Coefficient	0.04858	0.1330 ± 0.0357	0.1165 ± 0.221
		Global Efficiency	6.43 × 10 ⁻⁵	0.2099 ± 0.0113	0.2042 ± 0.0132
		Characteristic Path Length	8.60 × 10 ⁻⁵	5.5202 ± 0.3033	5.6622 ± 0.3765
	#1	Radius	0.003	7.4283 ± 0.4954	7.6601 ± 0.7407
		Diameter	0.04121	12.3051 ± 1.2286	12.8703 ± 1.5443
Max Modularity		0.04121	0.3654 ± 0.0213	0.3515 ± 0.0247	

4. Conclusion

Considering the important role of structural connections in the formation of subnetworks, the main conclusion is that using both structural and functional connections improve the study of brain connection abnormalities in schizophrenics. Examination of the data has shown that the path length parameters (characteristic path length, radius, and diameter) are greater in patients than in normal people. The result obtained, which is also consistent with the studies in the field, shows that in schizophrenia patients, the information interactions between the interconnected brain regions are slower. The greatest increase in path length parameters occurs in the jICA subnetwork #3 (Mostly including Somatomotor (SM) and visual areas in the brain based on Yeo Atlas) and subnetwork #2 (includes DMN) [3, 14]. This result shows that in schizophrenic patients, information interactions between interconnected brain regions are slowed down. On the other hand, the strength parameter in schizophrenic patients is lower than that in healthy people [14]. This change will create a significant difference between the healthy and the patients in the subnetworks, most of which are the visual and SM areas in the brain. As previously mentioned, changes in this parameter in schizophrenics indicate asynchronous connections of connected points in the brain [15].

In schizophrenia, the clustering coefficient is often reduced compared to healthy individuals. This result was also obtained in our data, and this parameter is lower in joint subnetwork #7, which mainly includes the areas SM, and in joint subnetwork #3 in patients compared to healthy people [16, 17]. From the changes in the parameters of the clustering coefficient compared with healthy people, it can be concluded that the organization of the brain network and the correct communication between neighbors as well as the complexity of a network are disturbed in schizophrenic patients [3]. Moreover, in our results, schizophrenic patients have lower global efficiency compared to healthy people, which is a factor for us to distinguish between healthy people and patients in joint subnetwork #1, which mainly includes limbic and DMN regions in the brain [18]. In our data, local efficiency is lower in schizophrenic people joint than in healthy people. This parameter accounts for the

largest difference between healthy people and patients in joint subnetworks #5, #7, and #3 [16, 17]. The change in local and global efficiency parameters indicates impaired parallel information transmission in the network and the average efficiency of the neighborhood subgraph of each node in our data is impaired in schizophrenic patients [18]. And the modularity parameter is lower in joint subnetworks #1, #4, and #9 of patients. These patients are expected to perform worse than healthy people in solving cognitive tasks [18]. And in ICA subnetworks path length parameters (characteristic path length, radius, and diameter) are greater in patients than in normal people. the strength parameter in schizophrenic patients is lower than that in healthy people. In our data, the clustering coefficient, and local and global efficiency are often reduced compared to healthy individuals. These results are consistent with other studies. In addition, we realized that by decomposing the brain system into multiple subsystems one is able to study psychotic disorders such as schizophrenia in more detail. Thus, changes in brain connections can be detected using graph parameters and subnetworks that are most sensitive in schizophrenia. More specifically, by studying subnetworks in these disorders, we can better diagnose the disorders of the patients and the way the connections change in these patients, which was not possible by studying the whole brain of these people. On the other hand, knowing the significant parameters in each subnetwork improves the personalization of diagnosis and treatment compared to a whole brain examination.


References

- 1- Sporns, O. "The complex brain: connectivity, dynamics, information." *Trends in Cognitive Sciences*, (2022).
- 2- Thomas Yeo, B., *et al.* "The organization of the human cerebral cortex estimated by intrinsic functional connectivity." *Journal of neurophysiology* 106(3): 1125-1165, (2011).
- 3- Liu, Y., *et al.* "Disrupted small-world networks in schizophrenia." *Brain*, 131(4): 945-961, (2008).
- 4- Zhu, J., *et al.* "Alterations of functional and structural networks in schizophrenia patients with auditory verbal hallucinations." *Frontiers in human neuroscience* 10: 114, (2016).
- 5- Keyvanfard, F., *et al.* "Interindividual Covariations of Brain Functional and Structural Connectivities Are

- Decomposed Blindly to Subnetworks: A Fusion-Based Approach." *Journal of Magnetic Resonance Imaging*, 51(6): 1779-1788, (2020).
- 6- Vergara, V. M., et al. "Altered Domain Functional Network Connectivity Strength and Randomness in." *Sec. Computational Psychiatry*, (2019)
 - 7- Sui, J., et al. "Function–structure associations of the brain: evidence from multimodal connectivity and covariance studies." *Neuroimage* 102: 11-23, (2014).
 - 8- JakubVohryzek, A.-G. Y. "Structural and functional connectomes from 27 schizophrenic patients and 27 matched healthy adults." *Zendo*, (2020).
 - 9- Hagmann, P., et al. "Mapping the structural core of human cerebral cortex." *PLoS biology* 6(7): e159, (2008).
 - 10- Honey, C. J., et al. "Predicting human resting-state functional connectivity from structural connectivity." *Proceedings of the National Academy of Sciences* 106(6): 2035-2040, (2009).
 - 11- Sui, J., et al. "Function–structure associations of the brain: evidence from multimodal connectivity and covariance studies." *Neuroimage* 102: 11-23, (2014).
 - 12- Mišić, B., et al. "Network-level structure-function relationships in human neocortex." *Cerebral Cortex* 26(7): 3285-3296, (2016).
 - 13- Cheng, P., et al. "Decreased integration of default-mode network during a working memory task in schizophrenia with severe attention deficits." *Frontiers in Cellular Neuroscience*, 16, (2022).
 - 14- Vergara, V. M., et al. "Altered domain functional network connectivity strength and randomness in schizophrenia." *Frontiers in Psychiatry* 10: 499, (2019).
 - 15- Messaritaki, E., et al. "Increased structural connectivity in high schizotypy." *Network Neuroscience* 7(1): 213-233, (2023).
 - 16- Zhu, J., et al. "Alterations of functional and structural networks in schizophrenia patients with auditory verbal hallucinations." *Frontiers in human neuroscience* 10: 114, (2016).
 - 17- Du, Y., et al. "Interaction among subsystems within default mode network diminished in schizophrenia patients: a dynamic connectivity approach." *Schizophrenia research* 170(1): 55-65, (2016).
 - 18- Cao, M., et al. "Topological organization of the human brain functional connectome across the lifespan." *Developmental cognitive neuroscience* 7: 76-93, (2014).



A Novel Generalizable Neural Decoder for Visual Object Recognition Using fMRI Data of Human Brains

Alireza Shakeripour¹, Poorya Aghaomidi¹, Shima Seyed-Allaei^{1,2}, Zahra Bahmani^{1*} 

¹Department of Computer and Electronic Engineering, Tarbiat Modares University, Tehran, Iran

²School of Cognitive Sciences, Institute for Research in Fundamental Sciences (IPM), Tehran, Iran

*Corresponding Author: Zahra Bahmani
Email: zabahmani@gmail.com

Abstract

Understanding the activity and functioning of various brain regions is a crucial aspect of neuroscience. Functional Magnetic Resonance Imaging (fMRI) has emerged as a powerful tool for recording brain activity during specific tasks, providing valuable insights into brain function. With advancements in machine learning and statistics, there is a growing potential to process and identify patterns in fMRI data. In this study, we aimed to decode the information embedded in fMRI data to recognize objects presented to subjects as visual images. We proposed a novel solution using deep learning techniques to develop a generalized model to address the limitations of previous subject-specific models. We introduced a specially designed transformer model for fMRI data, which not only exhibited superior spatial pattern recognition capabilities but also considered the relationships among different Regions Of Interests (ROIs) involved in visual processing. This approach ensured adaptability to differences in brain structure across different subjects. Our results demonstrated the potential for decoding visual images based on the brain activity of new subjects, thereby opening up a new way in reading the brain. The proposed decoder can be used in brain machine interface systems to help people with visual disabilities

Keywords: Functional Magnetic Resonance Imaging; Deep Learning; Object Recognition; Brain Decoding; Regions Of Interests Connectivity; Image Reconstruction.

1. Introduction

Computational neuroscience explores how sensory stimuli are decoded in nerve cells and investigates the potential of decoding information from neurons. Machine learning techniques have been increasingly used to read brain activities from fMRI data, primarily focused on object recognition. Understanding brain regions aids in diagnosing disorders and comparing results across individuals [1]. This study aims to improve the generalization of existing models. Image reconstruction from fMRI encounters challenges due to predictive coding, variations in neuronal responses, and factors like fatigue and attention. Although fMRI provides high spatial resolution, it indirectly captures aggregated neural activity through blood oxygenation [2, 3].

The challenges of building models based on data from multiple subjects arise from inter-individual variability in brain structure and function. While mapping brain structures can align general processing areas, they lack one-to-one functional correspondence, leading to limitations in image reconstruction that require more detailed patterns from different fMRI points. Variations in factors like blood pressure, mental state, and attention levels introduce statistical variations in fMRI responses, making current image reconstruction systems reliant on data from a single individual, limiting their applicability [4]. To address these challenges, this study proposes innovations including a transformer neural network that leverages attention to extract information from fMRI data, capturing relevant features in different visual regions of the brain and their interrelationships. The study also presents methods to enhance model generalization through assimilated input data, allowing evaluation on new individuals without the need for brain mapping or volume matching. By incorporating these advancements, the study aims to overcome limitations in brain decoding, making brain reading models more practical and applicable.

2. Materials and Methods

Existing methods for image reconstruction from fMRI data face challenges due to training and evaluating models on the same person's data. Inconsistencies in voxels, ROIs, statistical differences

in brain responses, and limited sample size contribute to these challenges. To overcome these limitations, we proposed a method that aims to create a generalized model capable of accommodating new individuals.

Our approach utilized a transformer neural network to address voxel mismatch and unify extracted information from fMRI data across different individuals. The model-building process involved two parts: feature extraction using a pre-trained network on the Imagenet image set (InceptionV3) and categorization using an MLP decoder. We employed a transformer network to extract features from fMRI signals, using the decoder to identify image components. The fMRI signal is inputted as vision-related areas, leveraging the transformer network's interconnection and attention capabilities. We handled fMRI signals from individuals with different brain sizes using an overlapping technique, eliminating the need for resizing or zero-padding. Our network had fewer training parameters, ensuring higher efficiency and faster model training, especially for large data volumes. This streamlined architecture enhanced the practicality and scalability of our method.

We conducted our study using the NSD dataset, which included fMRI signals from eight participants viewing images from the coco dataset. For training our network, we selected data from the first three subjects with varying voxel sizes. Using the HCP mask, we extracted 200 areas relevant to visual processing and adjusted their sizes for input into the network. From the images seen by these subjects, we focused on images containing person, resulting in a dataset of 26,888 images. The architecture of our model is shown in Figure 1.

3. Results

Our study achieved favorable accuracy in decoding visual images based on new subjects' brain activity using the proposed transformer model based on deep learning algorithms. The data was divided into three parts: train (80% of the total data), evaluation (10% of the total data), and test (10% of the total data). For the fMRI transformer network, the Cosine similarity metric was used as the evaluation metric, the similarity was 84.8% in train, 86.5% in evaluation, and 86.95% in test. The fully connected network, with features

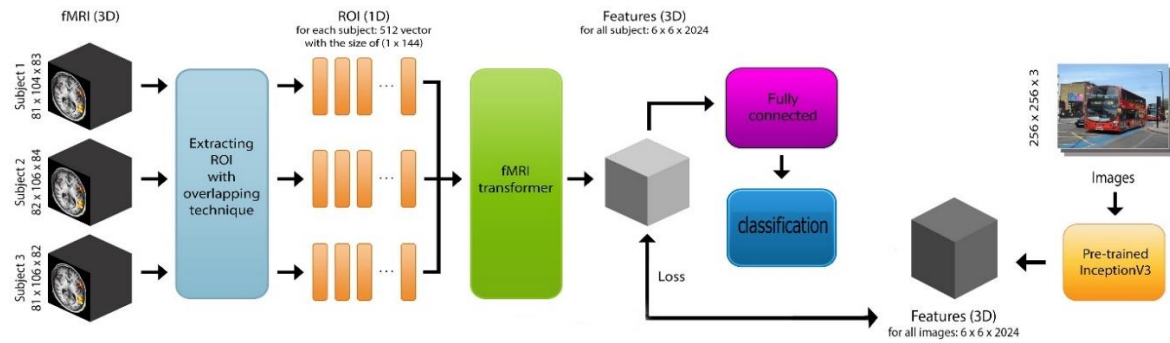


Figure 1. Model architecture

from the InceptionV3 network, achieved 75.6% accuracy in train, 72.8% in evaluation, and 71.6% in test. When using the fMRI transformer network's features, the accuracy was 73.1% in train, 72.3% in evaluation, and 70.3% in test. The accuracy achieved in the classification task further supported the effectiveness of our approach.

4. Conclusion

In conclusion, our study presents a novel approach using a transformer neural network and deep learning techniques to decode visual images from fMRI data. The results demonstrate the potential of our generalized model in accurately reconstructing images based on brain activity, offering promising prospects for advancing brain decoding research and its practical applications.

References

- 1- Bing Du, Xiaomu Cheng, Yiping Duan, and Huansheng Ning, "fMRI Brain Decoding and Its Applications in Brain-Computer Interface: A Survey." *Brain Sciences*, Vol. 12 (No. 2), p. 228, (2022).
- 2- Yukiyasu Kamitani and Frank Tong, "Decoding the visual and subjective contents of the human brain." *Nature neuroscience*, Vol. 8 (No. 5), pp. 679-85, (2005).
- 3- Kenneth A Norman, Sean M Polyn, Greg J Detre, and James V Haxby, "Beyond mind-reading: multi-voxel pattern analysis of fMRI data." *Trends in cognitive sciences*, Vol. 10 (No. 9), pp. 424-30, (2006).
- 4- Guy Gaziv *et al.*, "Self-supervised Natural Image Reconstruction and Large-scale Semantic Classification from Brain Activity." *Neuroimage*, Vol. 254p. 119121, (2022).



Application of Functional Connectivity Analysis in TMS Treatment Evaluation for Patients with Mental Disorder

Alireza Fallahi ^{1, 2*} , Hosna Tavakoli ³, Narges Hoseini-Tabatabaei ⁴, Reza Rostami ⁵, Hamid Soltanian-Zadeh ¹, Mohammad-Reza Nazem-Zadeh ^{3, 6}

¹ Control and Intelligent Processing Center of Excellence, School of Electrical and Computer Engineering, College of Engineering, University of Tehran, Tehran, Iran

² Biomedical Engineering Department, Hamedan University of Technology, Hamedan, Iran

³ Research Center for Molecular and Cellular Imaging, Advanced Medical Technologies and Equipment Institute, Tehran University of Medical Sciences, Tehran, Iran

⁴ Medical School, Tehran University of Medical Sciences, Tehran, Iran

⁵ Department of Psychology, University of Tehran, Tehran, Iran

⁶ Medical Physics and Biomedical Engineering Department, Tehran University of Medical Sciences, Tehran, Iran

*Corresponding Author: Alireza Fallahi
Email: fallahi@hut.ac.ir

Abstract

Psychoradiology is one of the new areas in neuroscience that aims to help diagnose and treatment of patients with neurological diseases using neuroimaging techniques. Transcranial Magnetic Stimulation (TMS) is a promising treatment modality for psychiatric and neurological disorders. Functional Magnetic Resonance Imaging (fMRI) as one of the main neuroimaging techniques, is a suitable method to reflect the functional integrity of the brain. Changes in Functional brain Connectivity (FC) are expected to provide potential biomarkers for the classification or prediction of brain disorders. In this paper, with the aim of helping people with mental disorders, we propose a neuroimaging-based method, using resting state MRI imaging and graph-based functional connectivity analysis. This method can be used in the field of medical diagnosis and specialized brain stimulation treatment with TMS to provide accurate and reliable medical services for radiologists and neurologists.

Keywords: Transcranial Magnetic Stimulation; Psychoradiology; Functional Connectivity; Graph Analysis.

1. Introduction

Mental diseases such as Schizophrenia (SZ), Bipolar Disorder (BD), and Major Depression Disorder (MDD) are a group of brain disorders that affect the thinking and behavior of a patient and cause discomfort for him. The cause of mental diseases is still not well known, because mental illnesses, like many diseases, do not have one known cause. Mental diseases are considered in the normal range of brain functions. While psychiatric disorders are diagnosed based on clinical interview symptom scores, there is no existing gold standard that can be used for definitive validation. Psychoradiology is a neuroimaging technique to help diagnose and treatment of patients with neurological diseases. Functional brain neuroimaging techniques including functional Magnetic Resonance Imaging (fMRI) [1, 2], Positron Emission Tomography (PET), and Electroencephalography (EEG) have become important tools in the investigation of brain diseases [3]. There is great hope that functional brain connectivity revealed using functional neuroimaging data can be useful to characterize abnormal brain function and, in turn, be useful for diagnosis and treatment [4]. Among various methods, fMRI enables non-invasive examination of brain function with high spatial resolution and is widely used to identify and characterize brain networks or connectivity among interconnected regions. Investigating differences in functional networks (or connectivity) between disorders such as SZ and BP may provide new insights into their disease mechanisms [5]. In addition, connectivity change criteria may be useful as biomarkers that can be used to classify individual patients using machine learning methods [4].

Various methods have been proposed to measure Functional Connectivity (FC) among brain regions using fMRI data [6-8]. While different approaches have different assumptions and advantages. Transcranial Magnetic Stimulation (TMS) is a Non-Invasive transcranial Brain Stimulation (NIBS) method that modulates neural activity by applying electromagnetic pulses to the scalp [9]. A unique strength of TMS is that it allows for in-vivo experimental investigation by depolarizing neurons to induce action potentials. TMS can be applied as single-pulse TMS (sTMS) or repetitive TMS (rTMS),

and rTMS is more commonly used as a treatment for neurological and psychiatric patients [10]. In this paper, we applied functional connectivity analysis to evaluate the effect of TMS treatment in BD and MDD patients. We used resting state functional MRI and applied network and graph-based analysis techniques.

2. Materials and Methods

2.1. Dataset and Data Preprocessing

This study included 20 mental disorder patients (10 BD and 10 MDD). After the patient's admission and the relevant psychological tests, structural and resting state functional MRI images are performed. MRI data were collected using a 64-channel phased-array head coil on a 3-Tesla scanner (Siemens Prisma, Erlangen, Germany) with software version "Syngo MR E11" at the Iranian National Brain Mapping Laboratory (NMBL). Anatomic images were acquired using a standard protocol including transverse T1 weighted images with Slice thickness = 4mm, TR/TE=5000/34 ms, 4 averages, matrix=128 × 128, 90-degree flip angle. The parameters for MPRAGE were the following: TR=1.9 s, TE=2.26 ms, FOV =250 mm, matrix =256 × 256, sagittal plane, slice thickness=1 mm, 176 slices. The rsfMRI images were acquired using Echo-Planar Imaging (EPI) protocol and the imaging parameters: Slice thickness=4 mm, 42 slices, TR=1.2 s, TE=30 ms, flip angle=90°, matrix 64 × 64, FOV=192 mm, total time= 6 min and 36 sec. All patients were asked to relax keep their eyes closed and think nothing in particular during the rsfMRI scanning process.

DPARF 4.3 (<http://rfmri.org/dpabi>; [11]) was used for the preprocessing of the rsfMRI data. For each subject, the first 10 time points were discarded. The remaining volumes were first corrected for the time difference between slices and then realigned to the middle volume for head-motion correction. Skull stripping was performed for a proper registration of functional images to T1-weighted images. Head movement was corrected using motion scrubbing. The resulting images were segmented into Grey Matter (GM), White Matter (WM), and Cerebrospinal Fluid (CSF), and then the mean BOLD signal was calculated from WM, CSF, and global signals (which is extracted from all voxels of the entire MRI volume) were

regressed on the rsfMRI data. Using the normalization parameters estimated by the T1 structural image, the realigned functional volumes (voxel size [3, 3, 3]) were spatially normalized to the Montreal Neurological Institute (MNI) space. Then using a Gaussian kernel (FWHM = 8 mm), the dataset was smoothed, linearly detrended, and temporally filtered (0.01– 0.08 Hz) to decrease the effect of low-frequency drifts. Using the Automated Anatomical Labeling (AAL) atlas [12], the volumes were segmented into 90 anatomical regions of interest (ROIs) to extract the ROIs time series. The mean time series of all voxels within the ROIs were used for the connectivity analysis.

2.2. Dataset Analysis

We applied functional network and graph-based nodal analysis as the neuroimaging methods for patient evaluation. The results of the analysis were applied to localize TMS field mapping and also follow-up patients after TMS treatment. We used the Yeo 7 functional network [13], as the one of main resting state functional atlases. These networks include; Default mode (DMN), Limbic (LIN), Visual (VIN), Frontoparietal (FPN), sensory-motor (SMN), Dorsal attention (DAN), and Ventral Attention (VAN). In each functional network the mean of within and between functional connectivity value, resulting from Pearson's correlation method, is calculated for network analysis. Graph-based nodal degree analysis [14] is also used as the other method for evaluating nodal alteration in patients with cognitive disease. In the network, the nodal degree is considered a basic and important measure of centrality and shows how a node interacts structurally and functionally with other nodes in the network. Then for each patient, these extracted measures were statistically compared with healthy normal group sample t-test. Then, based on these results and the individual characteristics of each patient, such as the type of illness, the affected area of the brain and even the head shape, the proper brain stimulation protocol is suggested for

TMS treatment. After treatment, the effectiveness of the proposed protocol is evaluated by these analysis. The block diagram of proposed protocol was shown in Figure 1.

3. Results

The results of brain network analysis, as well as nodal graph analysis, are shown in Figure 2 for MDD and BD patients. As seen in Figure 2a, before applying TMS in both cases, there is a lot of abnormal hypo connectivity between and within the brain functional networks. Figure 2b shows an effective reduction of abnormal connectivity after the TMS treatment process. These abnormalities are mostly limited to the limbic network in MDD patients and the DMN network in PD patients. Graph analysis also shows several abnormal decreases or increases in nodal degree before applying TMS that these abnormal nodes reduced after TMS treatment.

Figure 3 shows the head model and TMS field distribution method and Figure 4 shows for example how to distribute the field when the coil is on the right and left DLPFC area.

4. Conclusion

In this study, functional connectivity analysis is applied to investigate the effective features of cognitive networks of the brain in mental illness. Using proposed methods, it is possible to find changes in the functional and cognitive networks of the brain that have been disrupted by disease, which in some cases is difficult or impossible for expert neurologists. The proposed methods also make it possible to more accurately evaluate brain function in patients with mental illness and to evaluate the effectiveness of TMS treatment.

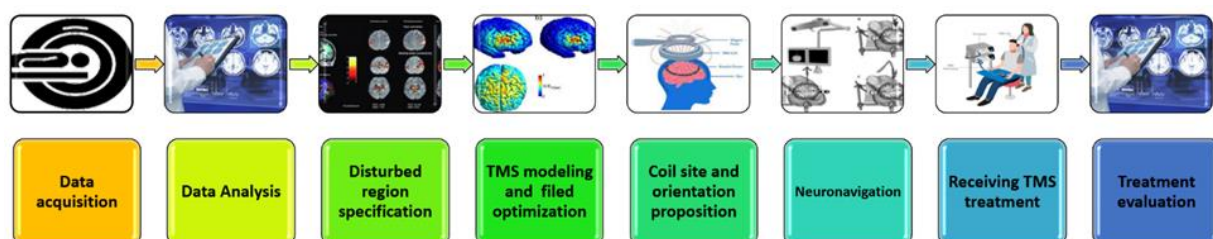


Figure 1. Block diagram of TMS treatment with neuroimaging analysis

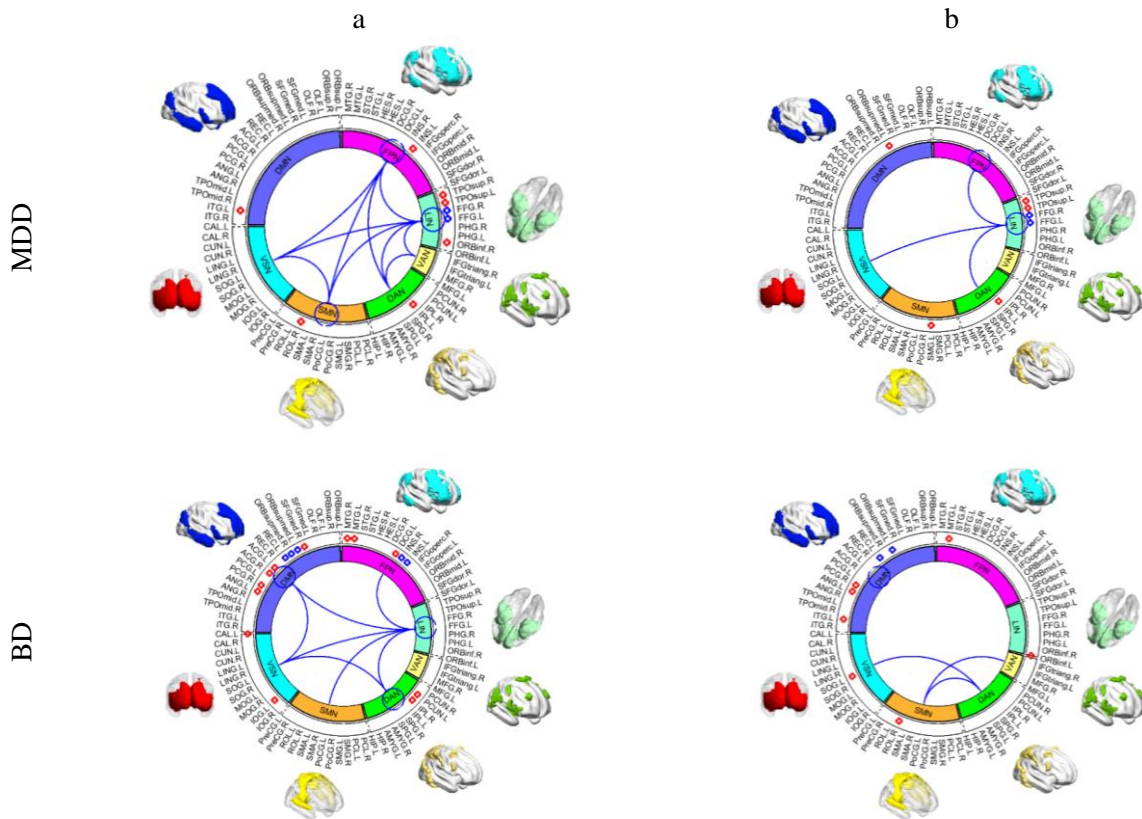


Figure 2. Result of functional network and nodal graph analysis. A: Before TMS treatment, B: After TMS treatment



Figure 3. Head model and TMS field distribution method

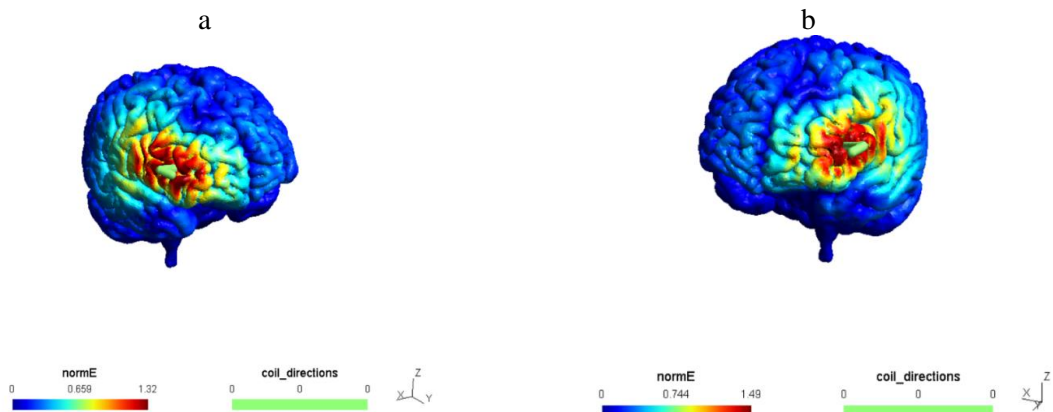


Figure 4. How to distribute the field when the coil is on the right (A) and left (B) DLPFC area

References

- 1- J.-H. Lee, T.-W. Lee, F. A. Jolesz, and S.-S. Yoo, “Independent vector analysis (IVA): Multivariate approach for fMRI group study,” *Neuroimage*, vol. 40, no. 1, pp. 86–109, Mar. (2008), doi: 10.1016/j.neuroimage.2007.11.019.
- 2- J. D. Power, B. L. Schlaggar, and S. E. Petersen, “Studying Brain Organization via Spontaneous fMRI Signal,” *Neuron*, vol. 84, no. 4, pp. 681–696, Nov. (2014), doi: 10.1016/j.neuron.2014.09.007.
- 3- A. Abi-Dargham and G. Horga, “The search for imaging biomarkers in psychiatric disorders,” *Nat. Med.*, vol. 22, no. 11, pp. 1248–1255, Nov. (2016), doi: 10.1038/nm.4190.
- 4- G. Deco and M. L. Kringelbach, “Great Expectations: Using Whole-Brain Computational Connectomics for Understanding Neuropsychiatric Disorders,” *Neuron*, vol. 84, no. 5, pp. 892–905, Dec. (2014), doi: 10.1016/j.neuron.2014.08.034.
- 5- B. Birur, N. V. Kraguljac, R. C. Shelton, and A. C. Lahti, “Brain structure, function, and neurochemistry in schizophrenia and bipolar disorder—a systematic review of the magnetic resonance neuroimaging literature,” *npj Schizophr.*, vol. 3, no. 1, p. 15, Apr. (2017), doi: 10.1038/s41537-017-0013-9.
- 6- M. van den Heuvel, R. Mandl, and H. H. Pol, “Normalized cut group clustering of resting-state fMRI data,” *PLoS One*, vol. 3, no. 4, (2008), doi: 10.1371/journal.pone.0002001.
- 7- S. M. Smith et al., “Functional connectomics from resting-state fMRI,” *Trends Cogn. Sci.*, vol. 17, no. 12, pp. 666–682, Dec. (2013), doi: 10.1016/j.tics.2013.09.016.
- 8- V. D. Calhoun and N. de Lacy, “Ten Key Observations on the Analysis of Resting-state Functional MR Imaging Data Using Independent Component Analysis,” *Neuroimaging Clin. N. Am.*, vol. 27, no. 4, pp. 561–579, Nov. (2017), doi: 10.1016/j.nic.2017.06.012.
- 9- A. M. Speer et al., “Opposite effects of high and low frequency rTMS on regional brain activity in depressed patients,” *Biol. Psychiatry*, vol. 48, no. 12, pp. 1133–1141, Dec. (2000), doi: 10.1016/S0006-3223(00)01065-9.
- 10- J.-P. Lefaucheur et al., “Evidence-based guidelines on the therapeutic use of repetitive transcranial magnetic stimulation (rTMS): An update (2014–2018),” *Clin. Neurophysiol.*, vol. 131, no. 2, pp. 474–528, Feb. (2020), doi: 10.1016/j.clinph.2019.11.002.
- 11- C.-G. Yan, X.-D. Wang, X.-N. Zuo, and Y.-F. Zang, “DPABI: Data Processing & Analysis for (Resting-State) Brain Imaging,” *Neuroinformatics*, vol. 14, no. 3, pp. 339–351, Jul. (2016), doi: 10.1007/s12021-016-9299-4.
- 12- N. Tzourio-Mazoyer et al., “Automated Anatomical Labeling of Activations in SPM Using a Macroscopic Anatomical Parcellation of the MNI MRI Single-Subject Brain,” *Neuroimage*, vol. 15, no. 1, pp. 273–289, Jan. (2002), doi: 10.1006/nimg.2001.0978.
- 13- B. T. Thomas Yeo et al., “The organization of the human cerebral cortex estimated by intrinsic functional connectivity,” *J. Neurophysiol.*, vol. 106, no. 3, pp. 1125–1165, (2011), doi: 10.1152/jn.00338.2011.
- 14- M. Rubinov and O. Sporns, “Complex network measures of brain connectivity: Uses and interpretations,” *Neuroimage*, vol. 52, no. 3, pp. 1059–1069, Sep. (2010), doi: 10.1016/j.neuroimage.2009.10.003.



A New Approach for Analyzing Functional Neuroimaging Data Using a Combination of CNN-LSTM and Occlusion Sensitivity Analysis to Identify Important Brain Regions in Visual Mental Imagery

Alireza Shafaei Darestani¹, Mohammad Asadpour^{1*} , Soomaayeh Heysieattalab²

¹Department of Computer Engineering, Faculty of Electrical and Computer Engineering, University of Tabriz, Tabriz, Iran

²Department of Cognitive Neuroscience, Faculty of Education and Psychology, University of Tabriz, Tabriz, Iran

*Corresponding Author: Mohammad Asadpour
Email: M_Asadpour@tabrizu.ac.ir

Abstract

Aphantasia is a condition that inhibits the ability to create mental images. In recent years, researchers have discovered a potential correlation between aphantasia and other mental health conditions, such as autism. However, due to the intricacy of the cognitive task, there is a debate among scientists about the specific regions of the brain that are causally involved in our ability to create mental images. The objective of this study is to present a groundbreaking deep learning framework for spatio-temporal analysis of block-designed fMRI signals. This framework, which we have named the classification and explanation deep learning framework for fMRI Signals (CEDLF-fMRI), has been designed to meet the complex needs of fMRI signal analysis. Our testing has demonstrated that CEDLF-fMRI outperforms traditional methods in classifying fMRI signals from complex experimental conditions. Furthermore, our framework generates a 3D image that provides an in-depth explanation of its decision-making process. Utilizing the generic object decoding dataset, the proposed CEDLF-fMRI demonstrated exceptional performance by classifying previously unseen samples at an impressive rate of 99% for two distinct categories: perception and imagery. Additionally, CEDLF-fMRI suggests that Right Lingual Gyrus (RLG) plays a key role in its ability to tell whether a signal belongs to imagery class or not.

Keywords: Aphantasia; Spatio-Temporal Analysis; functional Magnetic Resonance Imaging, Classification; Explanation; Deep Learning.

1. Introduction

Visual mental imagery refers to the ability of an individual to generate mental images in the absence of external stimuli. The assessment of visual imagery includes two critical factors: vividness and controllability. Researches have revealed that variations in these factors among individuals are associated with several mental disorders, including autism, schizophrenia, psychosis, and mood disorder [1-3]. Therefore, it is essential to understand the neural mechanisms underlying visual imagery to gain insights into the potential therapeutic interventions for these disorders. However, visual mental imagery tasks pose a challenge in cognitive neuroscience due to their complex nature. The inability of subjects to perform the task at an exact time point makes it difficult to monitor the process using modalities with low temporal resolutions, like fMRI. Moreover, the variable strength of visual imagery across individuals can result in a weak signal-to-noise ratio in modalities with higher temporal resolution, rendering traditional analysis methods ineffective.

Despite the aforementioned complexities, researchers have utilized diverse approaches to comprehend the cerebral basis of visual mental imagery. Thorudottir *et al.* conducted a study in which they compared four individuals who had suffered from bilateral Posterior Cerebral Artery (PCA) stroke. Surprisingly, only one of the patients had lost his ability for visual imagery. The researchers suggested that the patient's aphantasia was due to lesions in selective areas, specifically a small patch in the left fusiform gyrus and a part of the right lingual gyrus [4]. In a separate study, Spagna *et al.* conducted a large-scale meta-analysis of 46 fMRI studies, of which 27 investigated specifically visual mental imagery. They found that visual mental imagery engages fronto-parietal networks and a well-delimited region in the left fusiform gyrus [5].

In recent years, deep learning models have seen significant advancements in extracting spatial and temporal features from complex signals. Additionally, explainable artificial intelligence techniques have made it possible to understand the rational behind a model's decision-making process. The purpose of this study is to leverage these technologies to gain a better

understanding of the cerebral basis of visual mental imagery.

2. Materials and Methods

To gain insight into the cerebral basis of visual imagery, a comparison with visual perception is a helpful approach. As both processes share representations in multiple brain regions, the absence of deficits in perception among individuals with aphantasia suggests that certain brain regions may play a causal role in visual imagery without affecting perception. Therefore, we have used preprocessed block-designed fMRI data for three subjects from generic object decoding dataset [6] for analysis purposes. The dataset is composed of three different types of sessions: training perception, test perception, and test imagery. Each session is comprised of multiple runs, with each run containing multiple events. To compare visual perception and imagery, we combined images from the test perception and test imagery sessions. Subsequently, we filtered the events so that there were only two types in each image: stimulus and imagery. The scan per event was 3 and 5 for stimulus and imagery, respectively. We partitioned imagery events into three samples of three scans each with a stride of 1 for input dimension compatibility. The 3D fMRI volume was horizontally partitioned into ten batches, each containing five slices, to facilitate spatial feature extraction.

The CEDLF-fMRI model can be categorized into two primary components, namely classification and explanation. The first component involves three distinct stages, which are comprised of 3D Convolutional Neural Networks (CNN) for spatial feature extraction, bidirectional long-short term memory (Bi-LSTM) layers for temporal feature extraction, and Deep Neural Networks (DNN) for classification. Figure 1 illustrates the architecture of the classifier in detail. The second component of our approach consists of two stages aimed at providing an explanation for the classifier's decision. The first stage involves the removal of information contained within an Occluded Cube (OC) for all test samples. This is achieved by averaging voxel values inside the OC across time and samples. In the second stage, we assess the impact of the OC on the classifier's decision by computing the loss of the classifier with and

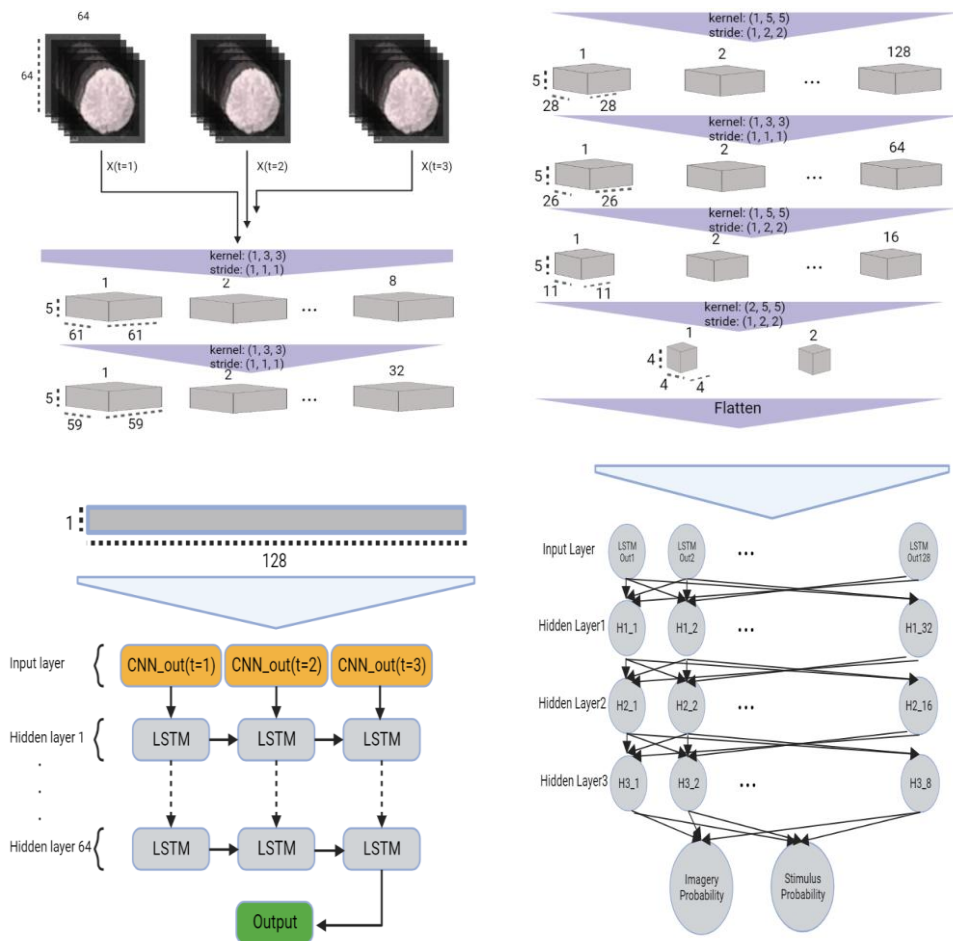


Figure 1. An illustration of the architecture of the classifier model

without this new OC included in the test set. This comparison allows us to infer the importance of the OC in shaping the classifier's output. The process of generating an explanation for the model's decision is illustrated in [Figure 2](#).

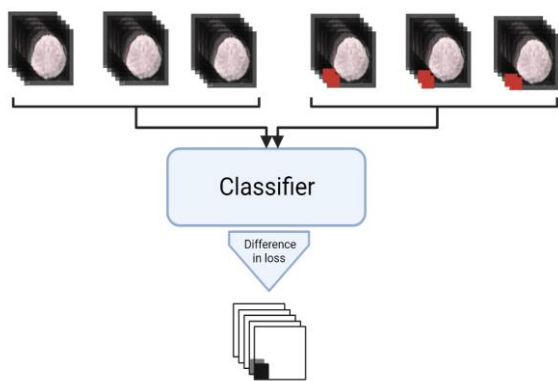


Figure 2. The process of generating an explanation

3. Results

In our evaluation of CEDLF-fMRI, we assessed its performance on previously unseen data from all five subjects. The classification accuracy varied among subjects across different axial batches. Notably, subject number 3 achieved the most accurate results, with an average accuracy of 99.9% across all axial batches. Additionally, the best axial batch across all subjects was identified as $z = (-45, -30)$ (Field Of View (FOV), $192 \times 192 \text{ mm}^2$; voxel size, $3 \times 3 \times 3 \text{ mm}^3$; slice gap, 0 mm; number of slices, 50). CEDLF-fMRI produces two statistical maps for imagery and stimulus classes. Regions with high z-scores for imagery indicate that removing information from that region resulted in the model misclassifying an imagery sample. Conversely, regions with low z-scores for imagery indicate that removing information from that region improved the model's ability to classify the sample as imagery. [Figure 3](#) shows an ortho view of z-score map for imagery class of subject 4.

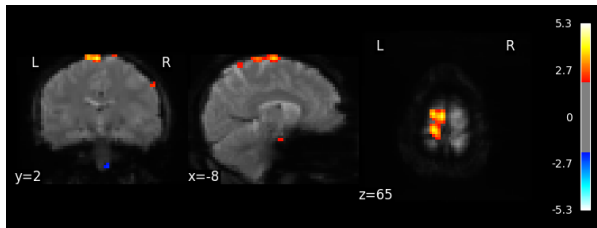


Figure 3. z-score map for subject 4

According to our analysis, several brain regions - such as the Right Fusiform Gyrus (RFG), Right Lingual Gyrus (RLG), superior parietal lobule (SPL), Ventral Pallidum (VP), Pre Central Gyrus (PreCG), Flocculonodular Lobe (FL), and Intra Parietal Lobe (IPL) - provide valuable information for the model's capability to detect imagery samples in the test set. Additionally, the findings demonstrate that the removal of information in the thalamus and posterior lobe of the cerebellum results in a loss of the model's ability to detect stimuli in the test set (Figure 4).

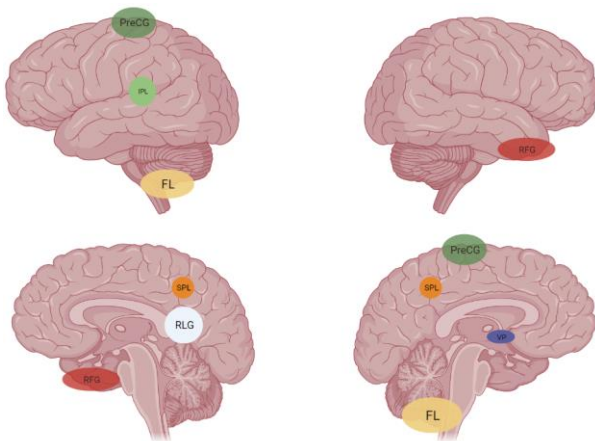


Figure 4. Brain regions that contribute the most to model's imagery identification ability

4. Conclusion

Identifying brain regions that are crucial in visual mental imagery holds immense significance, as these regions can act as potential indicators for various mental disorders. The primary aim of this study was to explore these significant regions by implementing cutting-edge technologies to address the intricacies of the cognitive task.

Based on the findings of this study, it can be concluded that there is consistency with prior research on visual mental imagery, indicating that several brain regions, including right lingual gyrus, and fusiform

gyrus play a critical role in this process. Moreover, the CEDLF-fMRI findings suggest that there are additional regions whose involvement in visual mental imagery was previously unknown.

References

- 1- C. J. Dance, M. Jaquiere, D.M. Eagleman, D. Porteus, A. Zeman, J. Simner, "What is the Relationship Between Aphantasia, Synaesthesia, and Autism?," *Consciousness and Cognition*, Vol. 89, Mar. 2021.
- 2- A. T. Sack, V. G. Van De Ven, S. Etschenberg, D. Schatz, D. E. J. Linden, "Enhanced Vividness of Mental Imagery as a Trait Marker of Schizophrenia?," *Schizophrenia Bulletin*, Vol. 31, Issue 1, Jan 2005.
- 3- S. A. Hales, C. Deeprose, G. M. Goodwin, E. A. Holmes, "Cognitions in Bipolar Disorder and Unipolar Depression: Imaging Suicide.," *Bipolar Disorders*, Vol. 13, Issue 7-8, Dec. 2011.
- 4- S. Thorudottir, H. M. Sigurdardottir, G. E. Rice, S. J. Kerry, R. J. Robotham, A. P. Leff, R. Starrfelt, "The Architect Who Lost the Ability to Imagine: The Cerebral Basis of Visual Imagery.," *Brain Sciences*, Vol. 10, Jan. 2020.
- 5- A. Spagna, J. Liu, P. Bartolomeo, D. HajHajate, "Visual mental imagery engages the left fusiform gyrus, but not the early visual cortex: A meta-analysis of neuroimaging evidence.," *Neuroscience and Behavioral Reviews*, Vol. 3 Jan. (2021).
- 6- T. Horikawa, Y. Kamitani, "Generic decoding of seen and imagined objects using hierarchical visual features.," *Nature Communications*, Vol. 8, May (2017).



An Eye Tracking Study: Effect of Audio on Video Ad Effectiveness

Ali Golbazi Mahdipour^{1*} , Shadi Ahmari², Asghar Ranjbar Aghdam³, Anahita Khorrami Banaraki^{4,5}

¹Neurobusiness Lab, Department of Business Administration and Engineering, School of Management, Economics, and Progress Engineering, Iran University of Science and Technology (IUST), Tehran, Iran

²Laboratory of Functional Neuroscience and Pathologies, Faculty of Medicine, York University, Canada

³Faculty of Management and Economics, Islamic Azad University, Science and Research Branch, Tehran, Iran

⁴Institute for Cognitive Science Studies, Tehran, Iran

⁵Brain and Cognition Clinic, Tehran, Iran

*Corresponding Author: Ali Golbazi Mahdipour
Email: ali.g.mahdipour@gmail.com

Abstract

This research aimed to evaluate the effect of audio in the performance of an audiovisual advertisement stimulus, using eye tracking technology and self-report measures.

31 participants (average age=24.2, SD=5.3) who were recruited for the experiment, watched the video ad without audio, and 30 other participants (average age=25.2, SD=8.8) watched the ad with the original audio. The eye movements of participants were recorded while they were watching the advertisement using a 30Hz Tobii eye tracker and Tobii Pro Studio software and were analyzed offline. Participants' self-report measures of effectiveness, affectiveness, perceptibility, and attractiveness were collected using 5-point Likert scales. Performing appropriate statistical tests, this study revealed a significant difference of attention in two investigated conditions. Significant results yielded for fixation count and visit duration of messages, visit duration of products, and total fixation duration of whole video ad. Yet no significant differences were found for self-report measures.

Neuromarketing methods like eye-tracking may provide useful information on the performance of video advertisement, which can be used for advertising effectiveness evaluation along with self-report techniques for more in-depth analysis.

Keywords: Neuromarketing; Aye-Tracking; Advertising; Marketing; Visual Attention; Audio-Visual Stimulation.

1. Introduction

Nowadays, with the development of cable networks and social media and ease of sharing videos online, people are exposed to more and more video advertisements [1]. Given the cost of creating video ads and publishing or broadcasting them in this jungle of advertisements, winning viewers' attention and effectively communicating marketing messages to customers has become a tougher marketing practice. Therefore, considering these difficulties, evaluating marketing stimuli before airing them seems to be a more vital move that companies should make.

Video ads are one of the most effective advertisement means, and have recently been the subject of more academic studies [2- 4]. However, an important part of video ads, which is audio, has yet to be studied more precisely. In this study, neuromarketing methods, which are among the most accurate and dependable methods for analyzing marketing stimuli, were used to evaluate the effect of audio on advertising effectiveness, along with traditionally used questionnaires.

Various electrophysiological devices and methods have been used in marketing and video advertisement studies, including FMRI, EEG, GSR, HRV, and eye-tracking [5]. Eye-tracking, which directly measures overt visual attention, has gained special attention among other methodologies for evaluating video advertisements [6]. Several researchers had used eye-tracking methods to study print ads by 1990 [7]. However, Aoki and Kenji of Tokyo Institute of Technology were the first academics to use eye-tracking methodology to scientifically evaluate video advertisements [8]. They proposed an analysis method for the cognitive attitude of a commercial film viewer. Two years later, Ale Smidts coined the term "neuromarketing" [9].

Earlier studies used recognition and recall tests to evaluate advertising methods, including video advertising [10]. After Aoki's work, more studies on video advertising were conducted using eye-tracking research. For instance, Siefert et al. compared viewers' attention to advertisements under fast forward and normal playing speed conditions in 2008 [11]. Later Feng, Cheung, Le Callet, and Ji used eye-tracking methods to reduce the need for conducting eye-

tracking experiments for evaluating video ad elements' saliency analysis in 2012 [12]. Despite these attempts to reduce the need for actually using eye-tracking technique in experiments, due to cultural and individual level variations eye tracking experiments have continued to grow in the field of video advertising effectiveness studies.

One of the key components of video advertising is audio, which plays a crucial role in conveying the message and capturing the attention of the audience [13]. A considerable body of literature has examined the impact of audio on various aspects of video advertising, such as attention, recall, and persuasion. Some studies have suggested that the addition of audio to video advertisements can enhance attention and recall, as it provides additional sensory cues that help to capture and retain the audience's attention [14]. Other studies have highlighted the potential for audio to increase persuasion in video advertising, as it can create emotional connections with the audience and enhance the message's impact [15]. However, the role of audio in video advertising is not always straightforward, and there are also studies that have suggested that audio can have negative effects on video advertising effectiveness. For instance, some research has highlighted that the use of background music in video advertising can distract the audience and reduce recall and comprehension of the message [16].

The aim of this study is to investigate the effect of audio on the performance of an audiovisual advertisement stimulus, using both eye tracking technology and self-report measures of effectiveness, affectiveness, perceptibility, and attractiveness. The study is designed to evaluate whether the presence or absence of audio in video advertising affects attention and other eye tracking measures, as well as subjective measures of advertising effectiveness. By using both objective and subjective measures, the study aims to provide a comprehensive understanding of the role of audio in enhancing or detracting from advertising performance.

2. Materials and Methods

2.1. Participants

Sixty-eight participants, most of whom were university students, were recruited for this research. Seven participants were excluded during the recording or analysis phase due to incomplete tests or insufficient recorded data. The study employed a non-probability random sampling method.

For the first phase of the experiments, 36 healthy Iranian participants were recruited, with four participants excluded from the study due to invalid data. Of the 31 remaining participants, 16 were female and 15 were male, with an average age of 24.2 (SD=5.3). The second group of subjects recruited for the second phase of the experiments consisted of 33 subjects, with three excluded due to incomplete tasks or invalid data. Fifteen of the participants in the second group were female, and the other half were male, with an average age of 25.2 (SD=8.8). All participants had normal or corrected-to-normal eyesight.

2.2. Material

The video ad selected for presentation in the experiments was a product-oriented ad for a well-known Iranian frying oil company. The original ad featured background guitar music and a narrative reading the ad messages, which were displayed as text on the video. The stimulus presented to the first group of participants was identical to the original ad, but without audio. The second stimulus presented to the

second group of participants was the original video ad. The stimulus had a length of 37 seconds, with a frame size of 1280x720 and a frame rate of 25 frames per second.

Following the video presentation, four questionnaires were sequentially presented on the computer monitor, asking participants to rate the attractiveness, effectiveness, affectiveness, and perceptibility of the advertisement they viewed.

2.3. Design

This research employed a two-sample between-subjects design, with both groups of participants presented with the same stimulus, except for its audio. The independent variable in this study was the audio of the video ad, while the dependent variables were the eye-tracking metrics and the self-reported attitudes of the participants towards the advertisement they viewed. The study was designed to enable a comparison of the eye-tracking and self-report measures between the two groups, as well as an investigation of the association between the eye-tracking metrics and self-report attitude towards the ad measure. The design of the stimulus presentation was recorded using Tobii Pro Studio software, as shown in Figure 1.

The questionnaires used in this research were designed in a five-point Likert scale format, resulting in the self-report data being of ordinal type. In contrast, the eye-tracking metrics were of scale type.

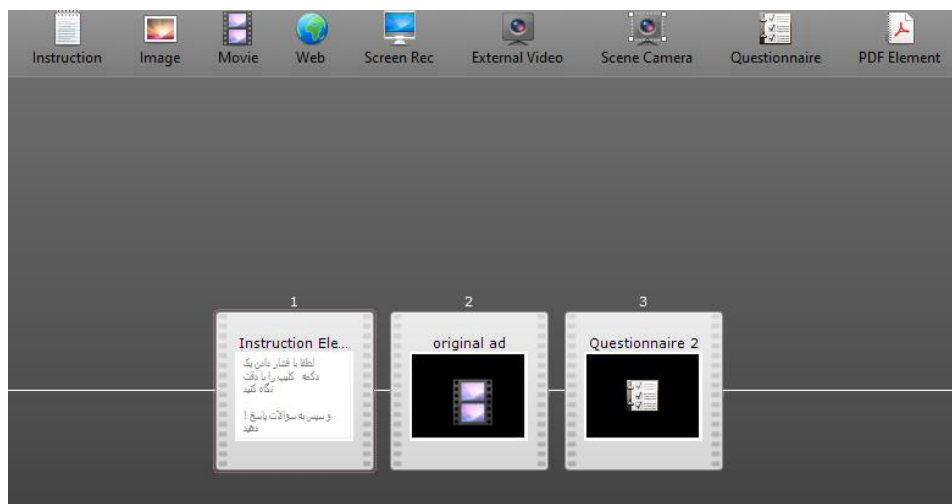


Figure 1. stimuli timeline of design and record tab in Tobii Pro Studio

2.4. Procedure

The procedure began by seating participants in a comfortable chair in a moderately lit room. After receiving an explanation of the experiment's safety and providing informed consent, the main experiment procedure commenced. Prior to stimulus presentation, participants performed a five-point calibration of the eye-tracking system. Participants were instructed to attentively watch the content displayed on the PC monitor and answer questions when prompted.

The first group of participants had their eye movements recorded while watching the video ad with its audio removed, followed by completing a questionnaire designed to obtain their self-reported attitude towards the ad. The second group of participants watched the original video ad while their eye movements were recorded.

2.5. Analysis

A total of 24 areas of interest (AOIs) were defined for each video, with seven AOIs corresponding to the products displayed in the ad, eight AOIs corresponding to the messages presented in the advertisement, eight AOIs corresponding to the faces of actors and actresses featured in the video, and one AOI defined for the entire area of the video displayed from start to finish. An example of the AOIs defined in the video is shown in [Figure 2](#).



Figure 2. A demonstrates how face AOIs were selected and B shows product and text AOIs

AOIs related to each of these four element categories were grouped together for further analysis. Eye-tracking metrics for each AOI group were calculated using Tobii I-VT Filter (Olsen, 2012), including Fixation Duration (FD), Total Fixation Duration (TFD), Fixation Count (FC), Visit Duration (VD), Total Visit Duration (TVD), and Visit Count (VC). These metrics were calculated for each AOI and AOI group and imported into the IBM SPSS software package (Nie, Bent, & Hull, 1975) for statistical analysis. Self-report measures of effectiveness, attractiveness, perceptibility, and affectiveness were also imported into SPSS for analysis.

3. Results

Statistical analysis proves some eye tracking metrics different for two conditions, yet self-report measures were not different for two conditions. The descriptive statistics for all eye-tracking variables are presented in [Figure 3](#).

Since most of the data were not normally distributed, we used non-parametric Mann-Whitney test to compare means of eye tracking metrics for two conditions, with and without audio. Results of this test indicated that Fixation Count on messages for the condition without audio was significantly greater ($U=313$, $p=0.028$), Visit Count on products was significantly greater for the condition with audio ($U=331$, $p=0.048$), Visit Duration on messages was greater for the condition without audio ($U=313$, $p=0.028$), Total Fixation Duration on the whole duration of video ad was significantly greater for the condition without audio ($U=2.000$, $p=0.000$). Eye tracking metrics on faces were not significantly different for the two conditions.

Kolmogorov-Smirnov test was used to compare means of self-report measures for two conditions. No statistically significant difference was yielded for affectiveness ($Z=0.803$, $p=0.541$), perceptibility ($Z=0.802$, $p=0.541$), effectiveness ($Z=0.395$, $p=0.998$), and attractiveness ($Z=0.273$, $p=1.000$).

The Squared Eta correlation was calculated in order to measure the strength of the relationship between self-report metrics and eye tracking metrics. See [Table 1](#) for the results of the tests.

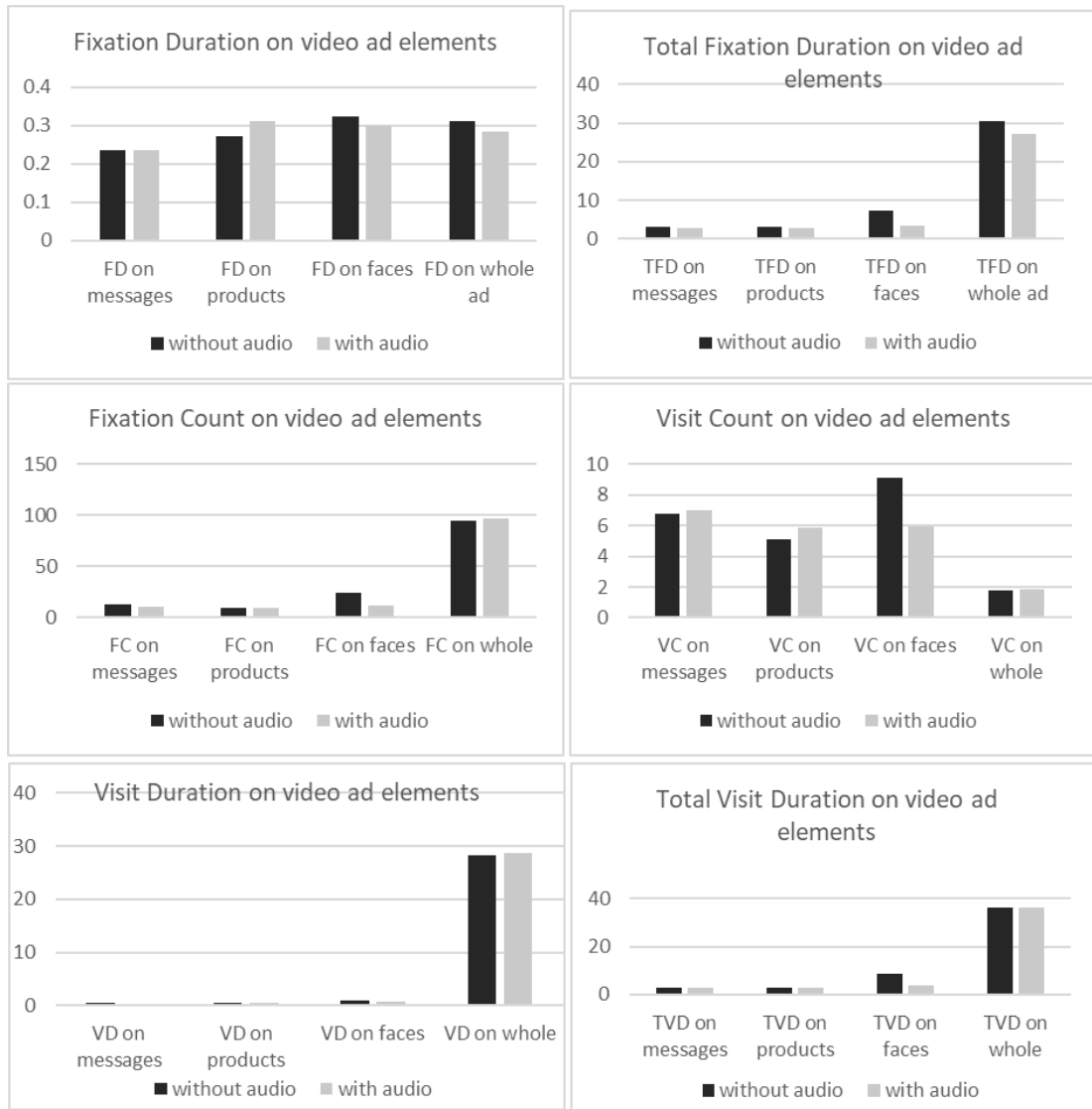


Figure 3. Descriptive statistics of eye-tracking metrics

4. Conclusion

This study shows that the self-report measures of higher-order metrics about video advertisement are not statistically different between the conditions with and without audio. However, the audio, including narrative and background music, affects the visual attention of viewers on different ad elements, including text messages and products presented in the ad. Additionally, the results of this research suggest that Total Fixation Duration and Total Visit Duration metrics can potentially be used to predict the attitude of viewers towards the advertisement.

Table 1. Squared correlation coefficient

whole video ad area				faces			
effectiveness		affectiveness		effectiveness		affectiveness	
metrics	η^2	metrics	η^2	metrics	η^2	metrics	η^2
FD	0.278784	FD	0.287296	FD	0.5329	FD	0.49
TFD	0.917764	TFD	0.913936	TFD	0.893025	TFD	0.927369
FC	0.6241	FC	0.599076	FC	0.183184	FC	0.192721
VC	0.120409	VC	0.088209	VC	0.171396	VC	0.108241
VD	0.627264	VD	0.717409	VD	0.765625	VD	0.715716
TVD	0.627264	TVD	0.717409	TVD	1	TVD	0.962361
attractiveness		perceptibility		attractiveness		perceptibility	
metrics	η^2	metrics	η^2	metrics	η^2	metrics	η^2
FD	0.379456	FD	0.439569	FD	0.492804	FD	0.4096
TFD	0.956484	TFD	0.919681	TFD	0.929296	TFD	0.813604
FC	0.651249	FC	0.755161	FC	0.126025	FC	0.284089
VC	0.047524	VC	0.125316	VC	0.142129	VC	0.123904
VD	0.724201	VD	0.767376	VD	0.6889	VD	0.7056
TVD	0.724201	TVD	0.767376	TVD	0.964324	TVD	0.992016
messages				products			
effectiveness		affectiveness		effectiveness		affectiveness	
metrics	η^2	metrics	η^2	metrics	η^2	metrics	η^2
FD	0.407044	FD	0.358801	FD	0.4489	FD	0.443556
TFD	0.974169	TFD	0.927369	TFD	0.893025	TFD	0.978121
FC	0.136161	FC	0.177241	FC	0.190096	FC	0.076176
VC	0.087616	VC	0.103041	VC	0.091204	VC	0.0529
VD	0.5329	VD	0.613089	VD	0.850084	VD	0.817216
TVD	0.937024	TVD	0.933156	TVD	0.8464	TVD	0.915849
attractiveness		perceptibility		attractiveness		perceptibility	
Metrics	η^2	metrics	η^2	metrics	η^2	metrics	η^2
FD	0.3969	FD	0.2809	FD	0.389376	FD	0.284089
TFD	0.978121	TFD	0.966289	TFD	0.839056	TFD	0.898704
FC	0.273529	FC	0.278784	FC	0.105625	FC	0.058081
VC	0.101124	VC	0.173889	VC	0.100489	VC	0.139129
VD	0.497025	VD	0.568516	VD	0.646416	VD	0.622521
TVD	0.9025	TVD	0.915849	TVD	0.9025	TVD	0.904401

References

- 1- Y. Liang, W. Liu, K. Liu, and H. Ma, "Automatic generation of textual advertisement for video advertising," in *2018 IEEE Fourth International Conference on Multimedia Big Data (BigMM)*, pp. 1–5, (2018).
- 2- C. J. S. Lourenço, G. Isabella, W. Verbeke, K. Vo, A. Dimoka, and R. P. Bagozzi, "How songs from growing up and viewers' attachment styles affect video ads' effectiveness," *Psychol. & Mark.*, vol. 40, no. 1, pp. 209–233, (2023).
- 3- S. Segev and J. Fernandes, "The anatomy of viral advertising: A content analysis of viral advertising from the elaboration likelihood model perspective," *J. Promot. Manag.*, vol. 29, no. 1, pp. 125–154, (2023).
- 4- L. Xiao, X. Li, and Y. Zhang, "Exploring the factors influencing consumer engagement behavior regarding short- form video advertising: A big data perspective," *J. Retail. Consum. Serv.*, vol. 70, p. 103170, (2023).
- 5- M. Nilashi *et al.*, "Neuromarketing: a review of research and implications for marketing," *J. Soft Comput. Decis. Support Syst.*, vol. 7, no. 2, pp. 23–31, (2020).
- 6- L.-A. Casado-Aranda, J. Sánchez-Fernández, E. Bigne, and A. Smidts, "The application of neuromarketing tools in communication research: A comprehensive review of trends," *Psychol. & Mark.*, (2023).
- 7- P. M. Fischer, J. W. Richards, E. J. Berman, and D. M. Krugman, "Recall and eye tracking study of adolescents viewing tobacco advertisements," *Jama*, vol. 261, no. 1, pp. 84–89, (1989).
- 8- H. Aoki and K. Itoh, "Analysis of cognitive attitudes to commercial films on basis of eye tracking data," in *Proceedings of the human factors and ergonomics society annual meeting*, vol. 44, no. 1, pp. 38–41, (2000).
- 9- A. Smidts, "Kijken in het brein: Over de mogelijkheden van neuromarketing," (2002).

- 10- C. Janiszewski, "The influence of nonattended material on the processing of advertising claims," *J. Mark. Res.*, vol. 27, no. 3, pp. 263–278, (1990).
- 11- C. Siefert, J. Gallent, D. Jacobs, B. Levine, H. Stipp, and C. Marci, "Biometric and eye-tracking insights into the efficiency of information processing of television advertising during fast-forward viewing," *Int. J. Advert.*, vol. 27, no. 3, pp. 425–446, (2008).
- 12- Y. Feng, G. Cheung, P. Le Callet, and Y. Ji, "Video attention deviation estimation using inter-frame visual saliency map analysis," in *Visual Information Processing and Communication III*, vol. 8305, pp. 140–147, (2012).
- 13- L. Simmonds, S. Bogomolova, R. Kennedy, M. Nenycz-Thiel, and S. Bellman, "A dual-process model of how incorporating audio-visual sensory cues in video advertising promotes active attention," *Psychol. & Mark.*, vol. 37, no. 8, pp. 1057–1067, (2020).
- 14- K. Hung, "Narrative music in congruent and incongruent TV advertising," *J. Advert.*, vol. 29, no. 1, pp. 25–34, (2000).
- 15- A.-K. Herget, P. Breves, and H. Schramm, "The influence of different levels of musical fit on the efficiency of audio-visual advertising," *Music. Sci.*, vol. 26, no. 1, pp. 3–23, (2022).
- 16- J. J. Kellaris and A. D. Cox, "The effects of background music in advertising: A reassessment," *J. Consum. Res.*, vol. 16, no. 1, pp. 113–118, (1989).



Cluster Level Inferences in Bilingual Resting State fMRI Dataset

Zahra Arab* , Vahid Nazmdeh, Mahsa Akhbari

Department of Biomedical Engineering, Science and Research Branch, Islamic Azad University, Tehran, Iran

*Corresponding Author: Zahra Arab
Email: arabzahra94@gmail.com

Abstract

Bilingualism is a skill that I can bring from childhood to adulthood. Few studies have been done on the brain structure of these people so far. In this article, with 56 resting state fMRI dataset including 28 subjects were native speakers of Mandarin Chinese living in the United States and the second 28 subjects were native speakers of Mandarin Chinese who lived in China, brain volume clusters were found for these people with $p\text{-FDR} < 0.005$ using the conn software. Each cluster compared to a known distribution of expected cluster sizes under the null hypothesis. at the end we got 8 cluster in compression group bilingual > control group.

Keywords: Resting State functional Magnetic Resonance Imaging; Bilingual; Cluster; Volume Base.

1. Introduction

Second language skills can be acquired from infancy to adulthood, so bilingualism is a useful model for examining neural brain changes that occur during a person's development [1]. According to neuroimaging research, it shows that bilingualism affects not only the shape and volume of the gray matter of the brain but also the white matter of the brain, indicating, for example, talented bilinguals display higher axonal density or myelination in white matter tracts that connect regions which can be critical for bilingual language processing, inclusive of the bilateral inferior frontal gyrus, the left advanced temporal gyrus, and the caudate nucleus [2-4].

One useful tool for investigating the brain's intrinsic functional networks by identifying similar patterns of shared functional activity between separate brain regions when the brain is not processing external stimuli is resting-state functional connectivity MRI. Among specific brain intrinsic functional networks, three networks are identified to be involved in cognitive control, of which language control is one factor. The frontoparietal network which incorporates the anterior prefrontal, the dorsolateral prefrontal, the dorsomedial superior frontal/anterior cingulate, the inferior parietal lobule, and the anterior insular cortex is this type of network [5].

2. Materials and Methods

The dataset contains the bilingual adult subset (in these case subjects are 19-38 years old) of the Reading Brain Project (RBP) data [6], 56 participants who 28 subjects were native speakers of Mandarin Chinese living in the United States (group a) and the second 28 subjects were native speakers of Mandarin Chinese who lived in China (group b). Resting state fMRI scanning was conducted using a 3T MRI scanner. After standard pre-processing according to pre-processing pipeline suggested by CONN for volume-based analysis, including realigned and unwrapped and correction and slice-time corrected and Artifact reduction tools usage and co-registration [7, 8] and therefore MNI segmentation and normalization using the SPM 12 [9].

In method, we survey the probability of clusters. This survey is done on each voxel and it must go above a threshold of this activity, and the connection of all voxels to form a cluster is done by checking the False Discovery Rate (FDR) of topological features. The search in the null hypothesis space for Finding the cluster by considering the threshold is called Gaussian processes. Suppose for the clustering of excursions for the set u and i are clusters and we have $i=1,\dots,c$ (Equation 1):

$$P(C_{\geq k_i, u} \geq 1) \quad (1)$$

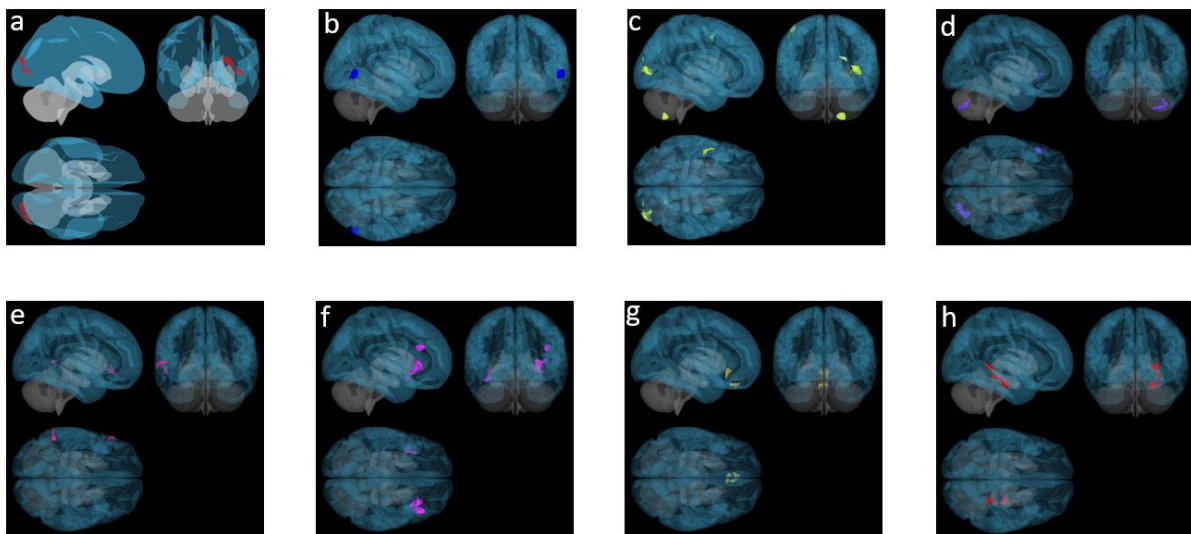


Figure 1. 8 clusters- cluster inferences in null hypothesis group a greater group b. In this form, the clusters may be in different areas or at a distance from each other, for example, “cluster c” contains several areas with different centers

This is the probability of cluster formation u , and the number of clusters in the set u has a volume equal to or greater than the cluster threshold value k that has a size equal to or greater than the clusters observed in c , and this must be greater than 1.

3. Results

As the result we got 8 cluster including a-h in Figure 1. Every size and location of them explained in Table 1. Condition of results is based on Cluster threshold: $p < 0.05$ cluster size p -FDR corrected and voxel threshold: $p < 0.001$ p -uncorrelated.

4. Conclusion

As in Li's article [5], the following regions are distinguished in terms of structure in people who have a second language in the reading task (Figure 2), in the findings of this research, comparing group a > group b, the following regions are present in the clustering. In fact, the effect of group a, which is bilingual people, on the brain regions seen in Figure 1 is shown. Here, active volumes were found using FDR and determining the desired threshold for activity. It was assumed that the activity of group 1 is more than group 2. It means that people who are bilingual are more active in these voxels and put in a one cluster. You can see multiple regions with their center are reported in Table. Like cluster d has two center of voxels (+32, -80, -46) and (-46, +22, 0) (Table 1).

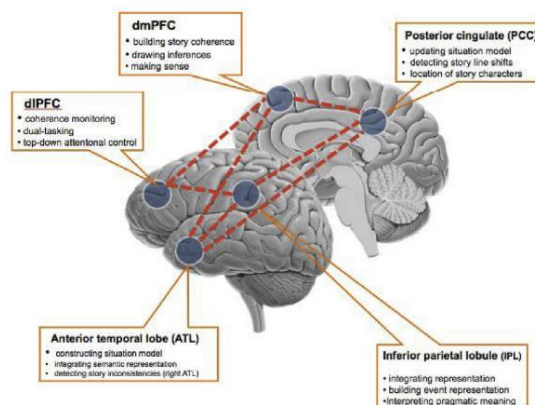


Figure 2. Key brain structures that support reading comprehension (based mostly on narrative text reading)

References

- Jonathan A Berken, Xiaoqian Chai, Jen-Kai Chen, Vincent L Gracco, and Denise Klein, "Effects of early and late bilingualism on resting-state functional connectivity." *Journal of Neuroscience*, Vol. 36 (No. 4), pp. 1165-72, (2016).
- Jonathan A Berken, Vincent L Gracco, Jen-Kai Chen, and Denise Klein, "The timing of language learning shapes brain structure associated with articulation." *Brain Structure and Function*, Vol. 221pp. 3591-600, (2016).
- Christos Pliatsikas, Elisavet Moschopoulou, and James Douglas Saddy, "The effects of bilingualism on the white matter structure of the brain." *Proceedings of the National Academy of Sciences*, Vol. 112 (No. 5), pp. 1334-37, (2015).
- Nandini C Singh et al., "Microstructural anatomical differences between bilinguals and monolinguals." *Bilingualism: Language and Cognition*, Vol. 21 (No. 5), pp. 995-1008, (2018).

Table 1. Cluster position and size and size p -FDR and size p -uncorrelated and peak p -uncorrelated

	Cluster (x,y,z)	size	Size P-FDR	Size P-Unc	Peak P-Unc
a	(+28,-96,+18)	344	0.0000230	0.000012	0.000009
b	(+60,-64,+2)	214	0.014089	0.000564	0.000006
c	(+44,-88,+2)	357	0.000937	0.000028	0.000019
c	(+18,-66,-60)	180	0.017227	0.001317	0.000000
c	(-44,-12,+58)	173	0.017227	0.001566	0.000059
d	(+32,-80,-46)	276	0.002736	0.000152	0.000005
d	(-46,+22,0)	136	0.037350	0.004150	0.000001
e	(-54,+26,-8)	159	0.033347	0.002528	0.000013
e	(-60,-48,+2)	144	0.033347	0.003705	0.000075
f	(+34,+18,-8)	308	0.003452	0.000102	0.000002
f	(-38,+10,-20)	200	0.017217	0.001013	0.000005
f	(+44,+24,+22)	180	0.018322	0.001617	0.000002
g	(-2,+38,-28)	328	0.001082	0.000057	0.000004
h	(+28,-40,-2)	402	0.000370	0.000011	0.000002

- 5- Ping Li and Roy B Clariana, "Reading comprehension in L1 and L2: An integrative approach." *Journal of Neurolinguistics*, Vol. 50pp. 94-105, (2019).
- 6- Ben Schloss Chun-Ting Hsu , Anya Yu ,Lindsey Ma ,Marissa Scotto , Friederike Seyfried, Chanyuan Gu "The Reading Brain Project L2 Adults. OpenNeuro. [Dataset] " (2021).
- 7- André Collignon, Frederik Maes, Dominique Delaere, Dirk Vandermeulen, Paul Suetens, and Guy Marchal, "Automated multi-modality image registration based on information theory." in *Information processing in medical imaging*, (1995), Vol. 3 (No. 6), pp. 263-74.
- 8- Colin Studholme, David John Hawkes, and Derek LG Hill, "Normalized entropy measure for multimodality image alignment." in *Medical imaging 1998: image processing*, (1998), Vol. 3338: *SPIE*, pp. 132-43.
- 9- John Ashburner and Karl J Friston, "Voxel-based morphometry—the methods." *Neuroimage*, Vol. 11 (No. 6), pp. 805-21, (2000).



Low-Quality Magnetoencephalography Data Reconstruction

Hanieh Arabian, Alireza Karimian * , Hamid Reza Marateb

Department of Biomedical Engineering, Faculty of Engineering, University of Isfahan, Isfahan, Iran

*Corresponding Author: Alireza Karimian
Email: Karimian@eng.ui.ac.ir

Abstract

Magnetoencephalography is a brain imaging method with high temporal-spatial resolution, whose data quality is reduced due to the failure of sensors. This study aimed to reconstruct the low-quality data of magnetoencephalography signals using surface reconstruction methods, partial differential equations algorithms, and finite element-based methods. To evaluate the performance of each method, R-square, root mean square error, and signal-to-noise ratio were calculated. The relation between these criteria was checked through proper statistical tests with a significance level of 0.05. The median method with mean and variance of R-square equal to 0.87 ± 0.03 was better than the other methods.

Keywords: Data Inpainting; Data Quality Enhancement; Magnetoencephalography; Signal Reconstruction.

1. Introduction

Electrophysiological activities in the human brain generate a weak magnetic field called Magnetoencephalography (MEG) in the spatial range of each active neuron. Combining the distribution of magnetic fields recorded by SQUID sensors with brain anatomy images can prepare a reliable functional map of active brain neurons. Magnetoencephalography has a better temporal-spatial resolution (1mm-1ms) compared to other imaging methods. Valuable information is lost and signal analysis is distorted by the low amplitude of a MEG signal compared to artifacts due to body, environment, or SQUID sensors. High-quality MEG signals are used to reconstruct neural sources and reveal interactions between different brain regions. So far, standard methods have been proposed for the inverse reconstruction of neural sources. Although the performance of each method has been acceptable in some cases, they have not had an acceptable response in the presence of combined noises [1, 2]. Considering that the number of active neurons is much more than the number of sensors; therefore, it is a serious problem to determine how to combine sources, spatial distribution, orientation, and periods when neurons are active. What is common in all of the studies, related to the reconstruction of neural sources, is the complete removal of noisy or low-quality channel data in the signal pre-processing stage [3, 4].

The studies have not considered the recovery and reconstruction of the lost signal of some MEG signal channels. Therefore, the recovery of this information is particularly important because noise reduction methods cannot reconstruct the signal of these channels. The importance of this research is lost in reducing the amount of information. Reconstruction of damaged or lost data can play an important role in a better understanding of brain interactions and disorders.

2. Materials and Methods

In this study, the magnetoencephalography signals of eleven healthy children with no history of brain disease registered at the Barcelona Children's Hospital were used and made available through a joint project in progress with us. 4D-Neuroimaging recording

device with 148 channels and a sampling frequency was 678.17 Hz. The duration of recording the signal was 10 minutes continuously and without interruption. Also, the position and orientation of each signal recording sensor were measured relative to the head center of the subject.

Since there was no gold standard for the data, to determine whether the data was intact or damaged, after dividing the signal of each channel into epochs of 500 milliseconds, they were visually examined by the researcher. After identifying intact epochs, some were randomly considered damaged epochs to be interpolated with the data from adjacent channels by 6 reconstruction methods. Image inpainting algorithms based on surface reconstruction, Partial Differential Equation (PDE), and interpolation algorithms based on Finite Element Method (FEM) were used to reconstruct the selected epochs by the signal of adjacent channels.

In two surface reconstruction methods, the mean and/or median of the 13 nearest neighbors were taken to reconstruct each selected epoch. In another method, after mapping the sensors from 3 dimensions to 2 dimensions, the modified Poisson equation was used as a PDE method with the help of 8 nearest neighbors' information of each sensor. In the FEM algorithm, four-node quadrilateral elements were used considering the 4 nearest neighbors.

After reconstructing the selected epochs, the performance of each reconstruction method was calculated by comparing the reconstructed signal with the original signal. To this, the R-square, Root Mean Square Error (RMSE), signal-to-noise ratio, Average Nearest Neighbor (ANN), Local Image Contrast (LIC), and the Percentage of the Outlier Border (POB) were calculated. The relation between the R-square, the RMSE, and the signal-to-noise ratio with the ANN, the LIC, and the POB with proper statistical tests and a significance level of 0.05 for each method were analyzed.

3. Results

After measuring the correlation coefficient and the level of significance of the relationship between the criteria of R-square and signal-to-noise ratio with the ANN and the POB using the bivariate Pearson

correlation statistical test, the P-value and the level of correlation for all selected epochs in all methods were more than 0.05 and less than 0.30, respectively. Then, to check the relationship between the R-square and the signal-to-noise ratio, and the LIC, using the bivariate Pearson correlation statistical test, the P-value and the correlation level for all the selected epochs in all methods were obtained less than 0.05 and more than 0.30, respectively.

The ratio of reconstructed epochs with an R-square greater than 0.70 to all of the reconstructed epochs, the average required time of an epoch reconstruction, and the average RMSE of the reconstructed epochs for each method are reported in Table 1.

Table 1. The statistics of different reconstruction methods

Reconstruction method	Percentage of reconstructed epochs with R-square ≥ 0.70	RMSE (Mean \pm SD)	Epoch reconstruction average time (μ s)
Mean	97.09	0.016 \pm 0.009	3.5
Median	99.33	0.016 \pm 0.009	5.9
Modified Poisson	52.80	0.021 \pm 0.005	665.9
FEM	59.29	0.236 \pm 0.813	2.9

4. Conclusion

For the modified Poisson equation, not only was the R-square ratio of the reconstructed epochs less than other methods (equal to 52.80%), but it also required a longer time (665.9 microseconds) to reconstruct an epoch. Among the other three methods, the mean and the median methods had the highest percentage of reconstructed epochs with an R-square greater than 0.70, equal to 97.09% and 99.33%, respectively. The average required time for mean and median methods was about 3.5 and 5.9 microseconds, respectively. Finally, the median method with the least average RMSE equal to 0.016 \pm 0.009 has recorded the best performance. The importance and innovation of this study is the damaged data reconstruction can be effective in reducing the elimination of data, and subsequently in increasing the results quality of neural sources inverse reconstruction.

Acknowledgments

We are very grateful for the cooperation of Professor Michael Angel Menanas (Polytechnic University of Catalonia-Spain) who provided pediatric magnetoencephalography signals and the University of Isfahan for financial support of this study.

References

- 1- Alain de Cheveigné and Dorothée Arzounian, "Robust detrending, rereferencing, outlier detection, and inpainting for multichannel data." *NeuroImage*, Vol. 172pp. 903-12 ,(2018).
- 2- Masashi Sato, Okito Yamashita, Masa-aki Sato, and Yoichi Miyawaki, "Information spreading by a combination of MEG source estimation and multivariate pattern classification." *PLOS ONE*, Vol. 13 (No. 6), p. e0198806 ,(2018).
- 3- Makoto Fukushima, Okito Yamashita, Thomas R. Knösche, and Masa-aki Sato, "MEG source reconstruction based on identification of directed source interactions on whole-brain anatomical networks." *NeuroImage*, Vol. 105pp. 408-27, (2015).
- 4- Alain de Cheveigné, "Sparse time artifact removal." *Journal of Neuroscience Methods*, Vol. 262pp. 14-20 , (2016).



Differentiation of Edematous, Tumoral and Normal Areas of Brain Using Diffusion Tensor and Diffusion Kurtosis Imaging

Yasaman Bastanipour ^{1*} , Mohammad Ali Oghabian ², Samira Raminfard ²

¹Department of Medical Physics and Radiology, North Khorasan University of Medical Sciences, Bojnurd, Iran

²Department of Medical Physics and Biomedical Engineering, School of Medicine, Tehran University of Medical Sciences, Tehran, Iran

*Corresponding Author: Yasaman Bastanipour
Email: Yasaman.bastanipour@yahoo.com

Abstract

Glioma is the most common type of intracranial tumor, and surgery followed by radiation therapy is the best treatment for high-grade glioma. Presurgical planning for glioma tumor resection and radiotherapy treatment require proper delineation of tumoral and peritumoral areas of brain.

Keywords: Glioma; Diffusion Kurtosis Imaging; Diffusion Tensor Imaging; Edema.

1. Introduction

Glioma is the most common type of intracranial tumor, and surgery followed by radiation therapy is the best treatment for high-grade glioma. Presurgical planning for glioma tumor resection and radiotherapy treatment require proper delineation of tumoral and peritumoral areas of brain. Studies have shown that advanced functional imaging can be useful to Differentiation of Edematous, Tumoral and Normal Areas of Brain. One of these methods is diffusion MRI (DWI), which investigates the diffusion of water molecules and the obstacles in their diffusion path. With advances in imaging protocols and analysis of diffusion images, it is possible to obtain parameters that express microstructural changes in brain tissue [1-3].

The objective of this study is to investigate the significance of various diffusion parameters, particularly the MK parameter, in differentiating between relapsed tumor regions, edematous regions, and normal regions (Figure 1).

2. Materials and Methods

13 patients with peritumoral edema underwent 3T multi-shell diffusion imaging with b-values of 1000 and 2000 mm^2 in 30 gradient directions. We fitted DTI and DKI to data in manually drawn regions of interest which were sized and matched to the MRS voxel and used their derived parameters (FA, MD, MK, and ADC) to characterize edematous, tumoral and normal brain areas. Initially, the assumption of normality of the data was rejected by the Shapiro-Wilk test. Therefore, non-parametric tests were used for group comparisons. The Wilcoxon test was used to determine the significance of the parameters between the three groups of relapsed, edematous, and normal. To determine significance, which means having a smaller p-value than 0.05, the parameters of ADC, MD, and MK were significantly different between the three aforementioned groups. The Mann-Whitney test was used to determine significance between the two groups of relapsed and normal, as well as between relapsed and edematous.

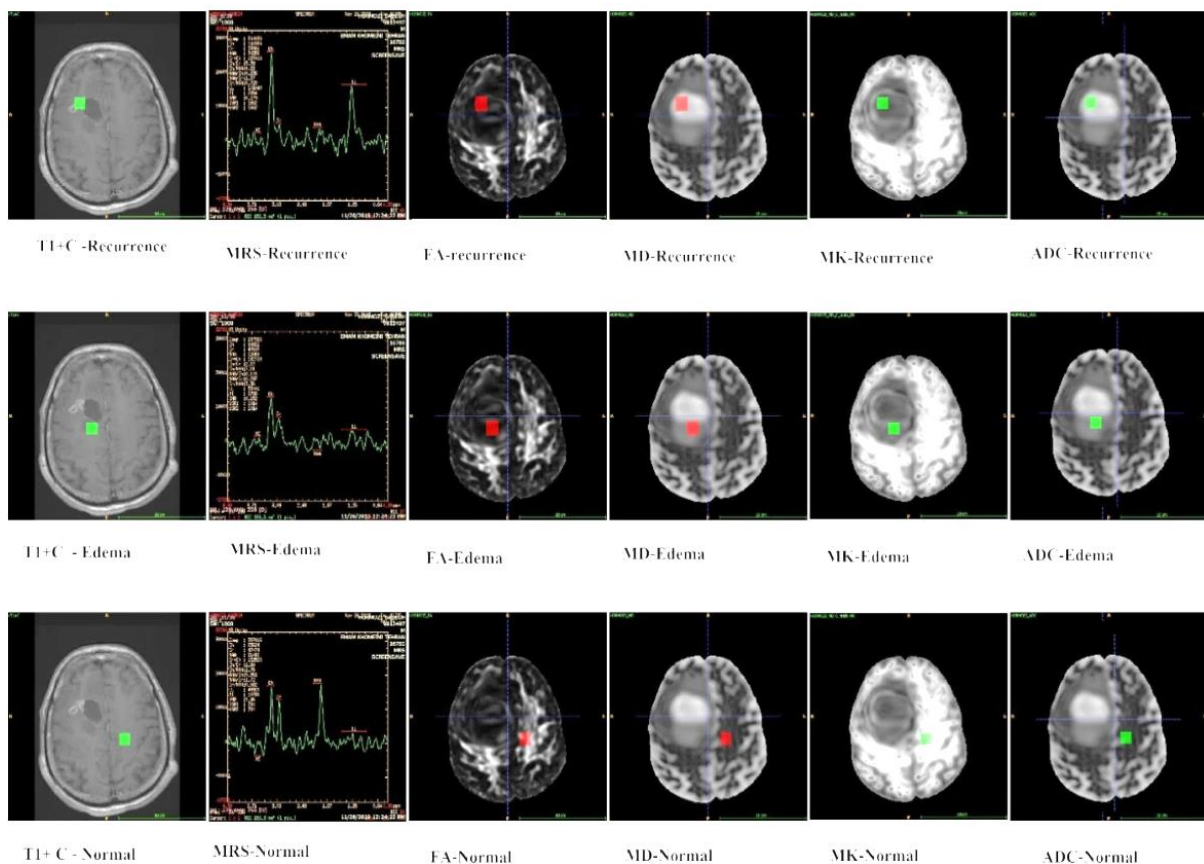


Figure 1. An example of ROI drawing of relapsed, edematous, and normal areas

3. Results

the parameters of ADC and MD were significantly different between the two groups of relapsed and normal, with a p-value of 0.041 ($p < 0.05$). Additionally, there was a significant difference in MK between the two groups of relapsed and normal, with a p-value of 0.02 ($p < 0.05$). The results of this study are reported in [Table 1](#).

4. Conclusion

The MK parameter has shown better potential than other diffusion parameters in distinguishing between relapsed and normal regions. As glioblastoma is a highly invasive tumor that can spread from the primary tumor site, the masks drawn in the edematous regions may contain some tumor tissue in addition to edema. As a result, there may be no significant difference in the mean diffusion parameters between the edematous and relapsed regions, as well as between the edematous and normal regions.

Therefore, none of the diffusion parameters under study may be able to differentiate between the edematous regions and other areas.

References

- 1- S Masjoodi, H Hashemi, MA Oghabian, and G Sharifi, "Differentiation of edematous, tumoral and normal areas of brain using diffusion tensor and neurite orientation dispersion and density imaging." *Journal of biomedical physics & engineering*, Vol. 8 (No .3) ,p. 251, (2018).
- 2- Pia C Sundgren, Q Dong, D Gomez-Hassan, SK Mukherji, P Maly, and R Welsh, "Diffusion tensor imaging of the brain: review of clinical applications." *Neuroradiology*, Vol. 46pp. 339-50, (2004).
- 3- S. Sinha, M. E. Bastin, I. R. Whittle ,and J. M. Wardlaw, "Diffusion tensor MR imaging of high-grade cerebral gliomas." (in eng), *AJNR Am J Neuroradiol*, Vol. 23 (No. 4), pp. 520-7, Apr (2002).

Table 1. Average studied diffusion parameters in three groups of relapsed, edematous, and normal regions

	Region	Count	Mean	S.D.	Median	p-value ¹	p-value ²	P-value ³	p-value ⁴
ADC	Recurrence	13	0.00164	0.00065	0.00150				
	Edema	13	0.00155	0.00055	0.00157	0.03	1.000	0.041	0.132
	Normal	13	0.00122	0.00037	0.00121				
FA	Recurrence	13	0.20	0.10	0.18				
	Edema	13	0.22	0.13	0.19	0.093			
	Normal	13	0.28	0.14	0.24				
MD	Recurrence	13	0.00163	0.00065	0.00151				
	Edema	13	0.00155	0.00054	0.00157	0.03	1.000	0.041	0.132
	Normal	13	0.00122	0.00036	0.00121				
MK	Recurrence	13	0.51	0.15	0.50				
	Edema	13	0.60	0.24	0.54	0.002	0.737	0.002	0.066
	Normal	13	0.76	0.21	0.73				

p-value¹: Wilcoxon Test, Comparison of three regions

p-value²: Adjusted Mann-Whitney Comparison between Recurrence And Edema Region

p-value³: Adjusted Mann-Whitney Comparison between Recurrence And Normal Region

p-value⁴: Adjusted Mann-Whitney Comparison between Normal And Edema Region



Dynamic Network Decoding of Working Memory Based on Electrophysiological Signals of Human Brain

Mahdiah Tahanejad, Zahra Bahmani * 

Department of Computer and Electronic Engineering, Tarbiat Modares University, Tehran, Iran

*Corresponding Author: Zahra Bahmani
Email: zabahmani@gmail.com

Abstract

The human brain consists of various parts, each with its own specific role in directing behaviors. Even simple tasks involve the coordinated activities of multiple brain regions. Cognitive activities, in general, rely on the ability to retain and adaptively manipulate information. This crucial capability is often attributed to Working Memory (WM). The current study aimed to gain a deeper insight into the neural mechanism of WM and understood how the neural activities were coordinated across brain regions. To achieve this objective, the invasively recorded electrophysiological activities from Medial Temporal (MT) cortex using high number of electrodes were analyzed. The human subjects did a verbal working memory task including three phases: encoding, maintenance and retrieval. Graphs of brain networks were generated using the Phase Locking Value (PLV), a functional connectivity metric, across six conventional frequency bands. In conclusion, a noteworthy observation was made regarding the reinforcement of a majority of brain connections during maintenance. Beta oscillations between the posterior and anterior hippocampus showed increased synchrony during maintenance of WM. This finding opens up the possibility of formulating a hypothesis regarding the flow of information between different brain regions during the maintenance state.

Keywords: Brain Connectivity; Working Memory; Maintenance; Phase Locking Value; Intracranial Electroencephalography.

1. Introduction

The disruption of brain oscillations and their synchrony is observed in various mental disorders, indicating their significance in normal brain function. These changes in neural synchrony not only contribute to understanding the underlying pathological mechanisms but also hold potential as a biological diagnostic method [1]. Early detection of these disruptions can aid in the development of effective treatments. Among the cognitive functions affected by these disorders, working memory stands out as a fundamental aspect. Disorders such as schizophrenia, bipolar disorder, autism disorder, attention deficit and hyperactivity disorder can be treated if we know about the neural mechanism of WM [2].

The increased phase locking between spikes and alpha-beta rhythms during WM in sensory areas was reported [3]. Besides an increased synchronous activities between frontal areas and temporal cortex was another clue of the role of brain oscillations during WM [4]. The recent studies showed that hippocampus was involved in coordination of WM induced brain activities. The maintenance of WM information was associated with heightened low-frequency activity in both the anterior and posterior hippocampus. Furthermore, they observed an increase in theta/alpha band phase synchronization (3 to 12 Hz) between the anterior and posterior subregions, indicating a correlation between WM and synchronized neural activity in these regions [1]. However, the exact mechanism of hippocampal formation remains elusive. In this study we want to address this issue using graph network methods based on signals simultaneously recorded from high number of electrodes.

2. Materials and Methods

The used database consists of iEEG signals of Medial Temporal cortex (MT) from 9 individuals with epilepsy (using in average 56 electrodes per subject). These individuals underwent implantation of depth electrodes in their MT lobe for therapeutic interventions. All participants had normal or corrected-to-normal vision and were right-handed. A verbal working memory task performed by these individuals involved the visual Sternberg test, which

comprised four states: fixation, encoding, maintenance, and retrieval [5].

Among the methods used to estimate functional connections, the "phase locking value (PLV)" was the most commonly employed. The analysis of recorded signals from each pair of electrodes involved several steps:

- 1- Preprocessing of iEEG signals to remove noise, artifacts, and extract signals in specific frames and frequency bands.
- 2- Quantification of the connection between pairs of iEEG channels using PLV metric. By employing "Equation 1", the PLV metric can be calculated between signals X and Y, considering parameters such as the number of time points (N) and the relative phase ($\Delta\varphi_{rel}$) between X and Y (Equation 1).

$$PLV(X, Y) = \left| \frac{1}{N} \sum_{n=1}^N e^{i\Delta\varphi_{rel}(t_n)} \right| \quad (1)$$

- 3- Determining appropriate thresholds to build a functional neural network. To determine significant PLV, a statistical comparison between PLVs and corresponded shuffled values was applied. This involved generating 50 trial-shuffled values for each electrode pair in each frequency and each period of task. The distribution of these permuted PLV values were then compared to the actual PLV values using a significance level of 0.02. Subsequently, the insignificant connections were removed based on this analysis.
- 4- To compare the state of maintenance and encoding periods, the values of PLV were normalized with respect to the fixation baseline state. The comparison was performed using a signrank statistical test at a significance level of 0.01.

3. Results

To investigate the difference between the distributions of the PLV values at Encoding-maintenance, we ran a statistical test after calculating the shuffle corrected PLV values for each stage of the working memory. As an example, Figure 1a shows the

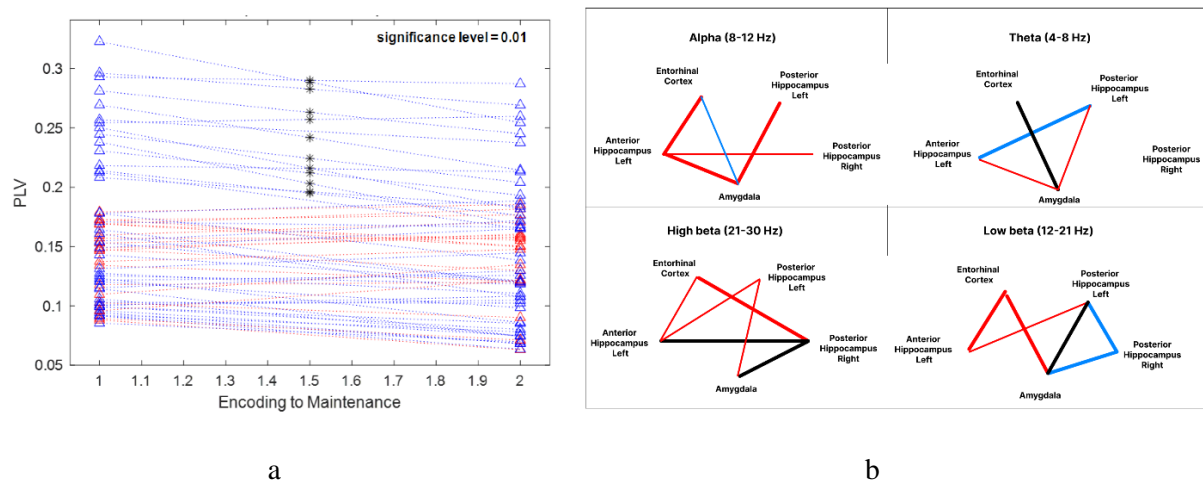


Figure 1. (a) the average PLV of all electrode pairs for the two areas Amygdala and Anterior Hippocampus Left in alpha (8-12 Hz) band, during the first session of the subject number 7. (b) PLV Comparison of Encoding and Maintenance States: five Brain Regions, six Frequency Bands. Red: Increased PLV in Maintenance. Blue: Decreased PLV in Maintenance. Black: Varied observations; with some individuals showed increased PLV while others exhibited a decrease. Line thickness indicates connection strength

average PLV of all electrode pairs for the two areas Amygdala and Anterior Hippocampus Left in alpha (8-12 Hz) band, during the first session of the subject number 7. Star signs were used to identify the significantly different values.

The maintenance of working memory at low frequencies (theta/alpha) involved the amygdala and both the anterior and posterior hippocampus, whereas higher frequencies (beta/gamma) show stronger connectivity between the posterior and anterior hippocampus, the cortical entorhinal junction, and the posterior hippocampus.

4. Conclusion

This article partially validates the previous study's findings on neural synchronization between the anterior and posterior hippocampus in the alpha/theta frequency band during information storage. Furthermore, the majority of frequency bands exhibit a closed-loop functional connection network, leading to the hypothesis that information circulates within the brain circuit while preserving its integrity. To confirm this hypothesis, a directed analysis of the network is required.

References

- 1- Ehsan Rezayat, Kelsey Clark, Mohammad-Reza A Dehaqani, and Behrad Noudoost, "Dependence of Working Memory on Coordinated Activity Across Brain Areas." *Frontiers in Systems Neuroscience*, Vol. 15, (2021).
- 2- Zahra Bahmani, Mohammad Reza Daliri, Yaser Merrikhi, Kelsey Clark, and Behrad Noudoost, "Working memory enhances cortical representations via spatially specific coordination of spike times." *Neuron*, Vol. 97 (No. 4), pp. 967-79. e6 ,(2018).
- 3- Ehsan Rezayat, Mohammad-Reza A Dehaqani, Kelsey Clark, Zahra Bahmani, Tirin Moore, and Behrad Noudoost, "Frontotemporal coordination predicts working memory performance and its local neural signatures." *Nature communications*, Vol. 12 (No. 1), p. 1103 ,(2021).
- 4- Vasileios Dimakopoulos, Pierre Mégevand, Lennart Stieglitz, Lukas Imbach, and Johannes Sarnthein, "Information flows from hippocampus to auditory cortex during replay of verbal working memory items." *bioRxiv*, p. 2021.03.11.434989 ,(2022).
- 5- Ece Boran *et al.*, "Dataset of human medial temporal lobe neurons ,scalp and intracranial EEG during a verbal working memory task." *Scientific data*, Vol. 7 (No. 1), pp. 1-7 ,(2020).



Attention Mechanism in GAT Network Can Decode Age from fMRI Data

Mahshad Faramarzi, Mansooreh Pakravan * 

Department of Electrical and Computer Engineering, Tarbiat Modares Univeristy, Tehran, Iran

*Corresponding Author: Mansooreh Pakravan
Email: mpakravan@modares.ac.ir

Abstract

Brain networks differ in connectivity and function at different ages. In this research, we use functional Magnetic Resonance Imaging (fMRI) data to extract functional brain connectivity based on correlation. Our aim is to classifying brain networks based on their age in 3 classes using Graph Attention Network (GAT). Our results show that brain graphs are well classifiable in 3 distinct classes (3-5 years, 7-12 years, and adults) by GAT network with validation accuracy=72% and test accuracy=62.5%.

Keywords: Functional Magnetic Resonance Imaging; Functional Brain Connectivity; Correlation; Graph Attention Network.

1. Introduction

The main aim of this study is to classify brain graphs with GNN based on their age. GNNs are a general framework for defining deep neural networks on graph data. The main idea of GNNs is to generate representations (embedding vectors) of nodes that depend on the structure of the graph as well as on the features of nodes. GNNs contain three important parts: 1) message passing 2) aggregation 3) update [1]. GAT network uses an attention mechanism to learn the importance of each neighbor for a given node. This allows the model to focus on the most relevant information, which can improve performance. GAT network is a GNN with special architecture constructed by several graph attention convolution layers based on attention. We expect GAT network can classify correctly brain graphs due to differences in the strength of region of interests (ROIs) connections at different ages [2].

Equation 1 represents a graph attention convolution layer where V_i^{k-1} and V_j^{k-1} represent the information (embedding vector) of i th node and the information of the adjacent nodes of i th node ($\mathcal{N}(i)$), respectively. superscript k is the index of network layer. In addition, $\alpha_{i,i}^{k-1}$ and $\alpha_{i,j}^{k-1}$ are attention weights for node i th information and it adjacent nodes, respectively. \sum operator is the aggregation part. The update part is summation of feature vectors of adjacent nodes and feature vectors of the main node. For the first layer, we use one-hot encoding vector for V_i^0 (all zero vector with only one 1 in i th element) and similarly for $V_j^0; j \in \mathcal{N}(i)$.

$$V_i^k = \alpha_{i,i}^{k-1} V_i^{k-1} + \sum_{j \in \mathcal{N}(i)} \alpha_{i,j}^{k-1} V_j^{k-1} \quad (1)$$

Equation 2 calculates the attention coefficients using softmax function. In fact, $e_{i,j}$ represents power of connection between nodes i and j . Furthermore, it's a scalar. Equation 3 calculates $e_{i,j}$ used in "Equation 2". $e_{i,j}^{k-1}$ is the output of LeakyReLU activation function. \parallel is concatenation symbol. W^{k-1} is the weights matrix of fully connected layer (trainable parameters). Vector a^{k-1} is multiplied by concatenated vector to turn it to a scalar and it also contains trainable parameters.

$$\alpha_{i,j}^{k-1} = \frac{\exp(e_{i,j}^{k-1})}{\sum_{k \in \mathcal{N}(i) \cup \{i\}} \exp(e_{i,j}^{k-1})} \quad (2)$$

$$e_{i,j}^{k-1} = \text{LeakyReLU} \left((a^{k-1})^T (W^{k-1} V_i^{k-1} \parallel W^{k-1} V_j^{k-1}) \right) \quad (3)$$

2. Materials and Methods

The fMRI data that are analyzed in this study include 122 children aged 3 to 12 and 33 adults aged 18 to 34 who watched passively a short movie while undergoing MRI scanner. We have used 25 ROIs to mask data similar to original study [3]; see Figure 1A. First, we calculated correlation matrix as graphs adjacency matrix and p-value of 25 BOLD signals (to hold only significant correlation coefficients less than 0.0001) for all subject. Correlation matrix of one of subjects is shown in Figure 1B. Second, we used GNN to solve classification task that is briefly shown in Figure 1C. We divided the data into three classes. Since the classes were unbalanced, we used random under sampling method to balance the classes. We randomly chose 33 subjects (33 is the size of the smallest class) from each class. Then we divided new dataset into test and train sets (number of test set = 24, number of train set = 75). After that we divided the train set into train and validation sets using k-fold cross validation (k=5) method. Figure 1D. shows the architecture of proposed network. This architecture includes three residually-connected graph attention layers, three ReLU activation functions, three batch norm layers, one pooling layer, and one fully connected layer. We used cross entropy loss as the loss function and stochastic gradient descent with nesterov and momentum=0.9 as optimizer in 183 epochs. Inputs of the architecture are 25-dimensional one-hot encoding vectors, i.e., the vector of i th node is an all-zero vector that only i th element is one (1st part of Figure 1D). The outputs of both primary layers are 64-dimensional vectors. We concatenated these outputs to use the extracted features of these layers in the input of third layer (2nd part of Figure 1D). In fact, our problem was graph level so that we turned the boosted graphs (3rd part of Figure. 1D) to vectors to classify by global mean pool layer (4th part of Figure 1D) which averages each vector along its rows. Furthermore,

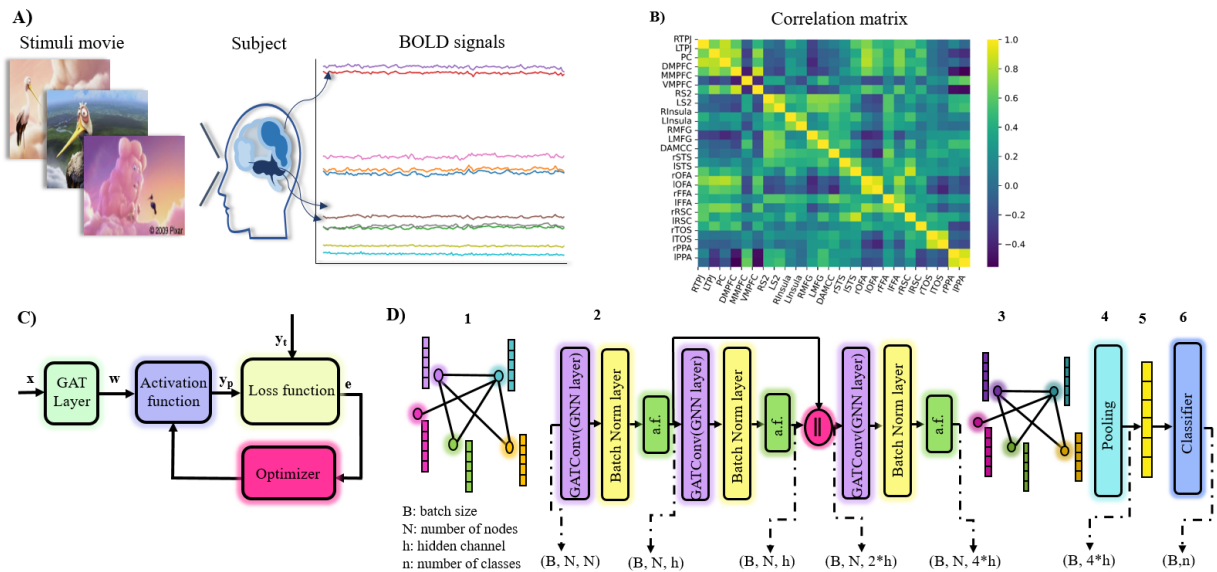


Figure 1. Summary of whole process. (A) Subjects watch passively a movie during fMRI recording; some BOLD signals of one of the subjects is shown; (B) Correlation matrix (adjacency matrix of brain connectivity graph) of one of the subjects; (C) Graph neural network problem (x is input vector, w is a trainable weight matrix, y_p is predicted label, y_t is true label, and e is the error); (D) Proposed Graph Attention Network: (1) One-hot encoding vectors of nodes. (2) Graph attention convolution layers (GNN layers) and activation functions. The purple part after second layer is a concatenation symbol. (3) Augmented, boosted, and final vectors. (4) Global mean pool layer. (5) A pooled vector. (6) Fully connected layer

these obtained vectors (5th part of Figure 1D) are inputs of fully connected layer. This layer classifies its inputs into three classes (6th part of Figure 1E).

3. Results

Confusion matrix of k-fold cross validation for validation data is shown in Figure 2A. Accuracy of these sets (75 samples) is equal to 72% (F1 score for class 3-5 years, 7-12 years, and adults are equal to 0.71, 0.60, and 0.78, respectively). Figure 2B shows accuracy of validation history. Accuracy of test set (24 samples) is equal to 62.5% (F1 score for class 3-5 years, 7-12 years, and adults are equal to 0.73, 0.56, and 0.53, respectively).

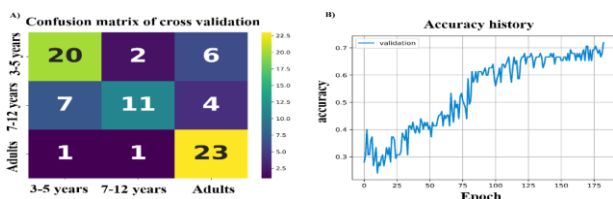


Figure 2. Summary of results. (A) Confusion matrix of validation sets. (B) Accuracy increase process versus epochs

4. Conclusion


Results show that proposed GAT network misclassify samples of 3-5 years class and 7-12 years class more which it means that the functional connectivity of these two classes are more similar than the functional connectivity of adults class. We can conclude that since movie watching highlights important states in brain network with respect to subject's age, then GAT network can decode age due to its attention mechanism.

References

- Chen, F., et al. "Graph representation learning: a survey." *APSIPA Transactions on Signal and Information Processing* 9: e15, (2020).
- Velickovic, Petar, et al. "Graph attention networks." *stat* 1050.20: 10-48550, (2017).
- Richardson, H., et al. "Development of the social brain from age three to twelve years." *Nature communications*, 9(1): 1027, (2018).



Automatic Driver Fatigue Detection using EEG Microstate Features

Zahra Yaddasht ^{1*} , Kamran Kazemi ¹, Habibollah Danyali ¹, Ardalan Aarabi ^{2,3}

¹Department of Electrical Engineering, Shiraz University of Technology, Shiraz, Iran

²Faculty of Medicine, University of Picardie Jules Verne, Amiens, France

³Laboratory of Functional Neuroscience and Pathologies, University Research Center, University Hospital, Amiens, France

*Corresponding Author: Zahra Yaddasht
Email: z.yaddasht@gmail.com

Abstract

Driver fatigue is a major cause of road accidents and automatic fatigue detection can help preventing these injuries. Electroencephalogram (EEG) microstate analysis has gained popularity as a tool for detecting brain state, mental workload and brain disease. The aim of this research is analyzing the EEG microstate features to effectively detect the driver fatigue state based on microstate features and Support Vector Machine (SVM) classifier. The global field power of EEG and its local maximum are calculated and then clustered in to four microstates. Four features were calculated for each segment of the data including duration, occurrence, time coverage and power. The extracted features in conjunction with SVM classifier have been used for automatic detection of fatigue state. The quantitative results based on leave-one-out approach using EEG data of 10 healthy subjects show that the proposed method has accuracy of 75%. To examine the optimal region of the brain and electrode selection, we divided the electrodes into four distinct regions and evaluated the accuracy of fatigue detection for each region. Our findings indicate that the central region yielded the best results.

Keywords: Driver Fatigue Detection Electroencephalogram; Microstate; Support Vector Machine.

1. Introduction

Mental fatigue affects driver's performance which posed threats to their safety. Frequently used methods of evaluating fatigue are based on physiological parameters such as ECG, EOG, and EEG signals [1]. EEG is widely used in studies, according to EEG characteristic, which is the fastest dynamic response of brain. EEG microstate is a new approach in analyzing EEG signals. Lehman *et al.* [2] proposed that EEG map topographies have quasi stable pattern. Their assumption is based on presence of single state for brain in a period of 60~120 milliseconds. They called it: "atoms of thoughts" or microstate. In this study we applied microstate analysis to extract microstate features consisting of duration, occurrence, time coverage and power for detecting fatigue and normal brain state. Finally, SVM classifier was used to validate the effectiveness of the proposed methods.

2. Materials and Methods

2.1. Subjects

Ten young healthy men participated in a driving simulation experiment. Five minutes of EEG recording was during normal state and five minutes was recorded during mental fatigue. The sampling frequency was 1000 Hz. These two five minutes divided in to 1sec segment. Considering all participants, we have 3000 segments for fatigue state and 3000 segments for normal state.

2.2. Methods

The block diagram of the proposed method is shown in Figure 1. The preprocessing includes 1-40 Hz filtering and removing baselines to eliminate the deviation of EEG signal. In this stage, the signal is filtered to four sub bands including 0.5~4, 4~8, 8~12 and 2-20 Hz.

2.3. Microstate Analysis and Classification

In the initial step, we calculated the Global Field Power (GFP) for each time point [3]. Next, we utilized the EEG topographies that corresponded to the maximum of GFP in the clustering algorithm. This was done under the assumption that EEG signals at the time point of GFP maxima have a relatively high signal-to-noise ratio. The polarity of each topography was disregarded. For each subject, we repeated the procedure while varying the number of clusters from 3 to 4. In the subsequent step, we obtained the group-level microstate classes by conducting a second clustering procedure. This was done using the topographies of microstates of each subject as clustering samples after the subject-level microstate analysis. Finally, we allocated EEG topographies at each time point to one of the mean microstate classes by determining the maximum spatial correlation coefficient between the topography of each time point and the group-level mean microstate maps. We calculated four features for each segment, including occurrence (i.e., the number of a given microstate per second), duration (i.e., the mean duration time of a microstate in seconds), coverage (i.e., the proportion of a given microstate), and mean power of each microstate in each segment. These four features were used for the classification of brain fatigue state via an

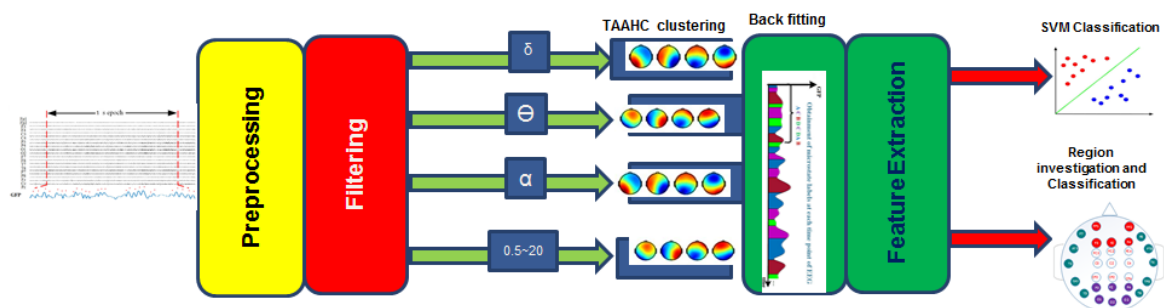
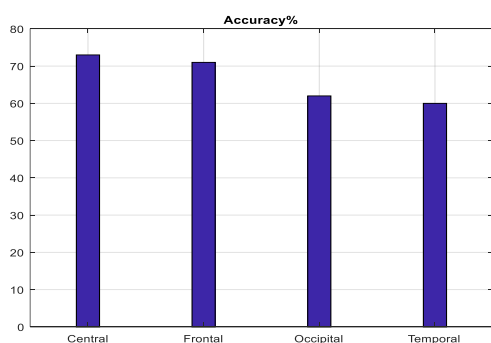


Figure 1. The block diagram of the proposed method for driver fatigue detection

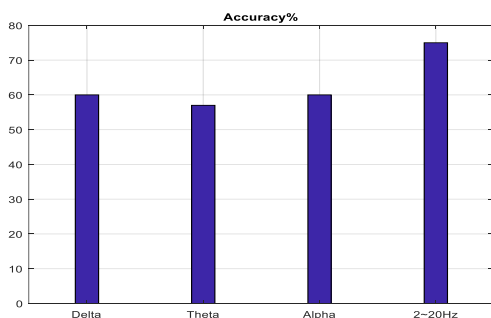
SVM classifier. Furthermore, we evaluated the impact of different brain regions, including frontal, central, occipital, and temporal, on classification accuracy.

3. Results

Figure 2 displays the average accuracy of the proposed classification method across different frequency bands (a) and various brain regions within the 2-20 Hz frequency band (b). Our results indicate that the best accuracy was achieved at 2-20 Hz when using all electrodes. Additionally, the central lobe exhibited higher accuracy as compared to the other lobes within the 2-20 Hz frequency band.



a



b

Figure 2. Accuracy of the proposed method for classification of driver fatigue using EEG. a) Classification using different EEG frequency bands, b) classification accuracy in different brain regions in 2~20 Hz

4. Conclusion

The results indicate that microstate features can be utilized to detect the fatigue and normal state of the brain. The addition of these features to classical ones, such as frequency features, may lead to improved

results. Furthermore, other classifiers, such as deep learning-based methods, have the potential to yield even better results. These assumptions could be investigated in future research.

References

- 1- Jiangxi Min *et al.* "driver fatigue detection through multiple entropy fusion analysis in an EEG-based system.", *PLOS ONE*. december (2017).
- 2- D. Lehmann, *et al.* "Brain electric microstates and momentary conscious mind states as building blocks of spontaneous thinking: I. Visual imagery and abstract thoughts." *Psychological*.vol29, no.1, pp1-11, jun(1998).
- 3- Kai Guan *et al.* "EEG Based Dynamic Functional Connectivity Analysis in Mental Workload Tasks With Different Types of Information" *IEEE transaction* VOL30, (2022).